IEEE Access
Multidisciplinary | Rapid Review | Open Access Journal

Received 27 May 2022, accepted 17 June 2022, date of publication 23 June 2022, date of current version 28 June 2022.

Digital Object Identifier 10.1109/ACCESS.2022.3185637

Overview of Approaches for Compensating Inherent Metamaterials Losses

BASHAR A. F. ESMAIL[1], (Member, IEEE), SLAWOMIR KOZIEL[1,2], (Fellow, IEEE), STANISLAW SZCZEPANSKI[2], AND HUDA A. MAJID[3], (Member, IEEE)

[1]Department of Engineering, Reykjavik University, 102 Reykjavík, Iceland
[2]Faculty of Electronics, Telecommunications and Informatics, Gdańsk University of Technology, 80-233 Gdańsk, Poland
[3]Fakulti Teknologi Kejuruteraan (FTK), Hab Pendidikan Tinggi Pagoh, Universiti Tun Hussein Onn Malaysia, Johor 84600, Malaysia

Corresponding author: Bashar A. F. Esmail (basharf@ru.is)

This work was supported in part by the Icelandic Centre for Research (RANNIS) under Grant 217771, and in part by the National Science Centre of Poland under Grant 2018/31/B/ST7/02369.

ABSTRACT Metamaterials are synthetic composite structures with extraordinary electromagnetic properties not readily accessible in ordinary materials. These media attracted massive attention due to their exotic characteristics. However, several issues have been encountered, such as the narrow bandwidth and inherent losses that restrict the spectrum and the variety of their applications. The losses have become the principal limiting factor when employing metamaterials in real-world applications. Consequently, overcoming them is crucially important and of practical necessity. This paper discusses the practical applications of metamaterials in constructing functional devices and the effects of the losses on such devices. In more depth, it reviews the available approaches for reducing the metamaterial losses developed over the last two decades in the light of available literature. These approaches include the utilization of the principles of electromagnetically induced transparency (EIT), geometric tailoring of the metamaterial structures, and embedding gain materials. Further, computational optimization techniques, such as particle swarm optimization (PSO) and genetic algorithm (GA), are also discussed to design low-loss metamaterials. The EIT-like metamaterial and the including of gain materials are systematic and universal approaches exhibiting low loss approaching zero. In contrast, the other two are not systematic and universal approaches.

INDEX TERMS Electromagnetically induced transparency (EIT), gain materials, metamaterial losses, optimization techniques.

I. INTRODUCTION

Metamaterials are synthetic composite structures, exhibiting extraordinary electromagnetic characteristics beyond natural materials, which is the reason to refer to them as metamaterials. Over the last two decades, metamaterials have attracted a significant attention in the engineering community because of their exceptional electromagnetic features, such as zero and negative index of refraction, artificial magnetism, inverse Doppler effect, and reverse Cherenkov radiation [1]–[6]. These properties are either missing in traditional materials or are difficult to be obtained at different frequency bands [7]. Metamaterials are ordered in repeating patterns (unit cells), at scales that are smaller than the operating wavelength. The extraordinary response of such materials, which concurrently provides negative permittivity (ε) and permeability (μ), was theoretically predicted by Victor Veselago in 1968 [8]. Three decades later, the effective medium theory was used by Pendry *et al.*. to construct such materials [3], [9]. The first artificial material structure, which consists of split-ring resonators (SRRs) and cut wires, was experimentally demonstrated by Smith *et al.*. in 2000 [10]. The exotic properties of this media are utilized in constructing many practical devices, such as super-lens and invisibility cloak [11]–[14]. Moreover, metamaterials were used in the sensing applications at different frequency spectrums, microwave [15], millimetre-wave [16], and terahertz [17]. Further, these artificial materials have found applications in the antenna field, where they are utilized to enhance the antenna performance in terms of improving directivity, gain, bandwidth, efficiency, minifying the size, and controlling the radiation pattern [18]–[23].

The associate editor coordinating the review of this manuscript and approving it for publication was Qi Luo.

The metamaterial properties have been enhanced through various strategies and procedures. However, some obstacles have been encountered, especially the cramped bandwidth and inherent losses limiting their practical applications. These media experience high losses, mainly when the operating frequency is boosted to a higher range, such as the millimeter-wave and terahertz spectra [24], [25]. These inherent losses can negatively impact the performance of the exotic characteristics of the metamaterials. They are stimulated by two components, which are the ohmic losses (i.e., the dissipation of energy due to the intrinsic ohmic loss of the metamaterial conducting layer) and radiation losses (i.e., metamaterials disperse the electromagnetic wave away from the incident wave) [26]. The latter is being a significant contributor to the overall losses. Metals are conventional conducting layers for building composite metamaterials. However, they experience high ohmic loss, even when using high conductivity metals such as silver or gold, which increases the losses that restrict the growth of devices based on metamaterials, especially at high frequencies [27]. Reducing the loss level is imperative for many applications expected from metamaterial technology, including perfect lenses, electromagnetic cloaks, absorbers, etc.

The losses are not limited to those induced by the conducting layer, where the design itself can bring substantial losses, such as radiation and resonant losses [28]–[32]. The resonant loss is induced by increasing the operating frequency. In contrast, the dominant component of the losses, the radiation losses, are due to the incident wave being dispersed away by the metamaterial elements. If the surface current of the structure is not distributed uniformly, the electric dipole moment is induced, thereby exhibiting high radiation loss [33]. The low loss property and the broad bandwidth are the factors to be considered when designing device-based metamaterial at a high-frequency range, such as the millimeter-wave and terahertz spectra. Over the last two decades, the researchers have proposed diverse approaches to mitigate the metamaterials losses at different frequency spectra, such as using the EIT, geometric tailoring of the unit cell, integrating active/gain materials, and using computational optimization techniques like PSO and GA [34]–[37]. Many reviews were published to discuss the applications of metamaterials in various fields. The applications of such media in enhancing the antenna performance were discussed in [38], while only one antenna feature, gain, was reviewed based on different metamaterial characteristics in [20]. The tuning strategies of metamaterials and their fascinating advantages were studied in [39]. To the best of our knowledge, no reported survey has been carried out in the literature to discuss metamaterials losses. This work provides the latest overview of the diverse techniques available to alleviate such losses.

Although metamaterial devices promise many revolutionary applications, they suffer from drawbacks of narrow bandwidth and inherent losses that restrict the variety of their applications. The high losses are the main barrier in designing efficient metamaterial devices, where they limit the application of metamaterial cloaks and cause difficulties in achieving perfect imaging and absorbers. Consequently, overcoming them is crucially important and of practical necessity. The available loss alleviation approaches need to be investigated, discussed, and compared to increase the knowledge of such an essential topic in the metamaterial field. Further, knowing all loss sources, ohmic, resonant, and radiation, is instrumental in realizing high-performance devices. Designing such media with low-loss property is a challenging task, which requires complete knowledge of the mitigations loss approaches, all loss sources, and factors affecting the design of each approach. The motivation of this work is to provide a complete review of available reduction loss techniques and compare their performance to be a guideline when designing low-loss metamaterial devices. This paper provides a state-of-the-art survey and a design guideline that considers the theoretical principles and practical limitations. In specific, the significant contributions of this review are as follows,

- The comprehensive background of metamaterial devices in terms of the design principles, limitations, and the impact of the inherent loss on their performance are presented. Further, all loss sources (ohmic, resonant, and radiation) and the factors affecting the design of low-loss metamaterials are investigated and discussed.
- Detailed analysis of the state-of-the-art theory and design of low loss metamaterials. Here, the available approaches (EIT, geometric tailoring, embedding gain materials, and computational optimization techniques) to alleviate/compensate the losses are investigated, discussed, and compared.
- Comprehensive comparison between loss reduction approaches highlights the advantages and drawbacks of each technique.
- Various observations concerning the metamaterial losses and their effects on constructing the functional devices are highlighted and summarized.

The remnant of the paper is organized as follows. The effective medium concept of metamaterials is presented in Section II. Section III introduces the functional devices based on metamaterials. The concept of metamaterial losses and the various approaches used for compensating such losses at various frequency bands are elaborated on in Section IV. In particular, it includes a detailed review of the four approaches used in the available literature to mitigate these losses. In particular, it includes a detailed review of the four approaches used in the available literature to mitigate these losses. Section V concludes the paper.

II. AN EFFECTIVE MEDIUM CONCEPT OF METAMATERIALS

As mentioned earlier, the interest in metamaterials increased considerably after using the effective medium model by Pendry *et al.* at low frequencies to induce electric and magnetic resonances [3], [9]. Then, the first metamaterial

structure consisting of a metallic wire and SRR with simultaneously negative ε and μ, was experimentally demonstrated by Smith *et al.*. in 2000. In composite materials, such as metamaterials which consist of more than one component, the electromagnetic properties are usually discontinuous at the interface of various components. Nevertheless, if the average size of the unit cell is significantly smaller than the free space wavelength, metamaterials can be considered an effective medium [9], [40]. Thus, they can be described by continued effective medium parameters; the effective permittivity (ε_{eff}) and effective permeability (μ_{eff}). The ε_{eff} and μ_{eff} based on the conventional structure, metallic wire and SRR, are expressed as follows [9], [10], [41]:

$$\varepsilon_{eff}(\omega) = 1 - \frac{\omega_p^2}{\omega(\omega + \frac{i\varepsilon_0 a^2 \omega_p^2}{\pi r^2 \sigma})} \tag{1}$$

$$\mu_{eff}(\omega) = 1 - \frac{F\omega^2}{\omega^2 - \omega_0^2 - i\omega\Gamma} \tag{2}$$

where $\omega_p$and σ are the plasma frequency and the metal conductivity, respectively. ε_0 is the permittivity of the free space, whereas $a(r)$ is the period (radius) of the metallic wire. F is the area ratio of SRR to unit cell, and ω_0 and Γ are specified by the geometry and the parameters of the SRR. Different methods for reconstructing the constitutive parameters (ε and μ, and refractive index) were proposed in the literature [42], [43]. In these methods, these parameters can be obtained from the complex S-parameters.

III. METAMATERIAL DEVICES

The effective medium concept was the base in the metamaterial research over the last two decades. The constitutive parameters can be tailored by adjusting the geometrical parameters of the metamaterials, resulting in fascinating phenomena. Several functional devices have been implemented and improved based on metamaterial's exotic and extreme properties. The most interesting one is the invisibility cloak, which was proposed theoretically by Pendry *et al.*. [44] and verified experimentally by Schurig *et al.*. in 2006 [45]. The 2D cross-section of the metamaterial cloak is shown in Fig. 1(a), in which the medium is invisible for electromagnetic radiation in a specific frequency range. The first practical metamaterial cloak device was developed based on the transformation optics approach [see Fig. 1(b)] [45]. In this report, the cylindrical cloaking device was based on conventional SRRs with a different distribution of μ_{eff}. Another exciting device-based metamaterial is the super-lens. As it is well known, the resolution of the traditional lenses is restricted by the diffraction limit, where the evanescent wave fades exponentially during propagation, and it cannot reach the image plane. To solve this, the metamaterial with a negative refractive index can be used as a lens to improve the near-field evanescent wave distributed by the object. In brief, an evanescent wave converges and propagates further in the negative refractive index materials compared to the positive-index materials, as shown in Fig. 1(c) [46]. The theoretical

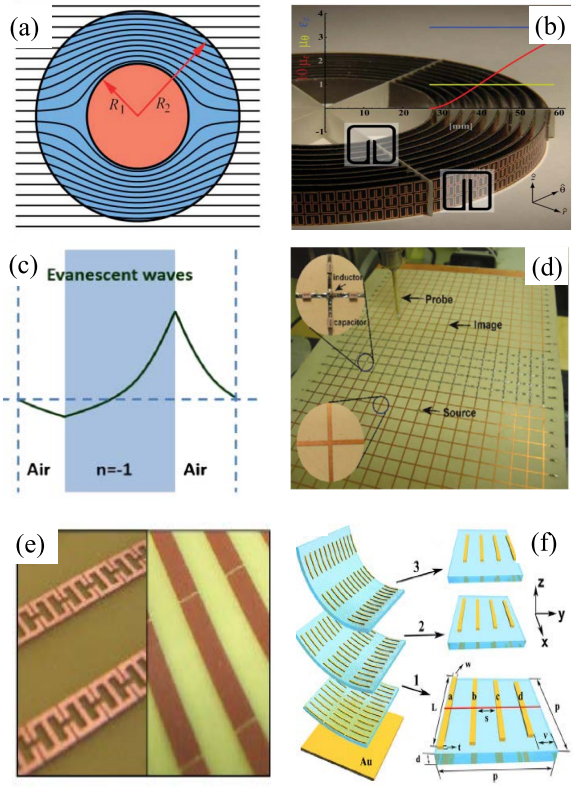

FIGURE 1. Common practical devices based on metamaterials: (a) 2D cross-section of invisibility cloak based metamaterial [44], (b) photograph of a microwave cylindrical cloaking device based on SRRs with a different distribution of effective permeability [45], (c) the evanescent wave is augmented and goes further in negative refractive index materials [46], (d) photograph of the first experimental metamaterial lens, the top and bottom insets referred to the negative and positive refractive index shapes, respectively [47], (e) both sides of the first experimental metamaterial absorber [48], and (f) schematic view of a stacked structure of 3 × 3 broadband metamaterial absorber at terahertz regime; each unit cell consists of four metallic bars [49].

base of the metamaterials lens was introduced by Pendry [46]. In this report, the negative refractive index medium with $\varepsilon = \mu = -1$ acted as a perfect lens. The first experimental lens-based metamaterials was proposed by Grbic and Eleftheriades cf. 1(d) [47]. Furthermore, these artificial materials are used as electromagnetic absorbers, which are highly demanded in many applications. Landy *et al.* [48] experimentally demonstrated the first perfect metamaterial absorber, cf. Fig. 1(e). However, the narrow bandwidth and polarization-sensitive limit the practical application of such a design. Later, many metamaterial absorbers with broad bandwidth were reported at different frequency spectra. The broadband terahertz metamaterial absorber was reported in [49], which consists of three layers of different geometries to obtain a broad absorption property over 0.5 THz [see Fig. 1(f)]. It is worth mentioning that these materials were used to build other practical devices, such as filters, sensors, electromagnetic converters, electromagnetic concentrators, shielding, and lens antennas [50]–[55].

The inherent losses and narrow bandwidth are the significant challenges that need to be addressed in the metamaterials

field, both seriously limiting their practical applications. High losses are the main barrier in designing efficient metamaterial devices. Such losses restrict the application of metamaterial cloaks and cause difficulties in achieving perfect imaging and absorber. Their reduction is instrumental in the development of high-performance metamaterial-based devices, especially at high frequencies.

IV. METAMATERIAL LOSSES

One of the significant challenges that need to be addressed in the field of metamaterials is their inherent losses, which are usually caused by the structure conducting layer, as well as the radiation scattering. The losses seriously restrict the practical application range of metamaterials. They are also a significant obstacle in designing efficient metamaterial-based devices. The metal used in the conducting layers of the metamaterial is not ideal, especially at the millimeter-wave and terahertz spectra. Therefore, the metallic layer loss is pivotal and must be considered during the design stage, especially at high frequencies [56]. The ohmic/intrinsic loss is defined as the total power consumed by the metamaterial due to resistive heating of the metallic layer. The inherent losses are not limited to those caused by the conducting layers. Other loss sources include the resonant [57] and radiation ones [58]. The resonant loss is induced by increasing the operating frequency to a higher range. The radiation loss, on the other hand, is the dominant component of the losses, which can be induced by dispersing electromagnetic wave away from the incident wave. Fig. 2 displays the ohmic and radiation losses. The electromagnetic wave is directed to the metamaterial from an external source, where part of it is dissipated inside the conducting layer of the structure. Another part, more prominent, radiates off the metamaterial, thereby inducing radiation loss. Various factors have been used to measure the metamaterial losses, such as the transmission coefficient, the surface current distribution, suitably defined figures of merit (FOM), and the imaginary values of the constitutive parameters [24]. The transmission, S_{21}, is used to measure the peak of the transmission band at the desired frequency, where the near-zero (in dB scale) or unity (in linear scale) shows low loss property. The FOM is defined as the ratio of the real to the imaginary parts of the refractive index, FOM= –Re(n)/Im(n) [59], [60]. The high value of FOM indicates a low loss property. Further, the imaginary values of the constitutive parameters (ε, μ, and refractive index) are also used to measure the loss, where their values should be zero or approaching zero at the frequency of interest to obtain a low loss structure [58]. Moreover, the structure with a high-quality factor (Q-factor) offers a low loss property, where it is expressed by $Q = (I/R) \times \sqrt{(L/C)}$. Several approaches were proposed in the literature to compensate for the metamaterial losses, such as inducing an EIT phenomenon, the proper geometrical arrangement of the structure, embedding the gain materials, and using the GA and PSO. The loss compensation approaches with their features are shown in Fig. 3.

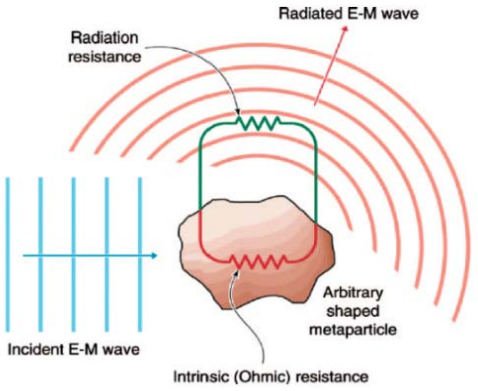

FIGURE 2. The inherent losses in metamaterials [23].

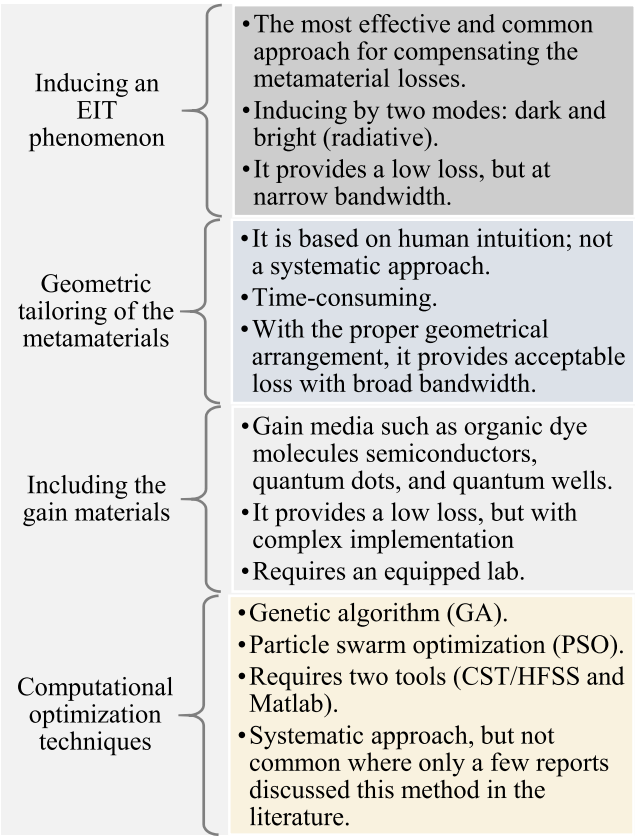

FIGURE 3. The loss compensation approaches with their features.

A. LOW LOSS METAMATERIALS BASED ON EIT

EIT is a charismatic physical phenomenon defined as a quantum interference effect that happens in the three-level atomic system, where the nontransparent atomic medium is introduced to be transparent in the very narrowband window within a broad absorption spectrum [61], [62]. This phenomenon can be employed to design low-loss metamaterials. However, its impact can only be stimulated by tailoring the geometrical parameters of structure components [61], [63]. Thus far, EIT is the most widely used approach for mitigating the metamaterial losses. By applying

its principles, two modes are induced, the dark and the bright (radiative) ones, generally by SRR and cut wire components of the conventional metamaterial. The strong coupling between the dark and the bright modes leads to a sharp transparency peak at the desired frequency. Here, the metamaterial components prompt obverse currents resulting in the destructive interference of the scattering fields, thereby repressing the radiation loss. Over the last decade, several metamaterials based on the EIT phenomenon were proposed to mitigate such inherent loss. The EIT significantly alleviates the radiation loss at different frequency regimes from microwave [64] to terahertz [58]. According to the available literature, the metamaterial losses are acceptable, and their unnatural properties can still be achieved at the microwave band. Nevertheless, the losses-based EIT phenomenon were extensively investigated for further enhancing the performance of the metamaterial-based devices at this band [64]–[75]. Most of the reports in the last decade discussed the losses of the conventional metamaterial structure: SRR and cut wire. Li *et al.* [64] proposed EIT metamaterial-based electric toroidal dipolar response for realizing a low loss. Such response was obtained by currents flowing on the surface of a torus along its meridians, in which the external electric field caused the electric toroidal dipolar response. The EIT metamaterial consists of an asymmetric split range resonator (ASRR) and cut wire operating as dark and bright modes. The two configurations and their transmission spectra are shown in Figs. 4(a)–(d), in which the transmission dips occurred at 8.12 GHz for both structures. When the ASRRs and the cut wire were combined, the destructive interference due to the strong coupling between the ASRR-EIT dark mode and cut wire-EIT bright mode leads to a sharp transparency transmission peak of 0.56 dB (0.88 in the linear scale) at 8.12 GHz. Figures 4(e) and (f) show the fabricated prototype of the EIT-like metamaterial and its transmission spectrum, respectively. To envision the coupling process of both structures, the surface currents of the two components were studied, in which the currents were out of phase, leading to cancelling each other and inducing a high transmission peak [see Fig. 4(g)]. Moreover, the imaginary values of ε and μ were approximately zero at 8.12 GHz [see Fig. 4(h)]. The overall dimensions of the unit cell are 0.43 $\lambda_0 \times$ 0.43 λ_0, where λ_0 refers to the free-space wavelength. The structure loss is still high despite inducing the EIT at a low-frequency range. Zhang *et al.* [66] proposed two mirrored double-gap split-ring resonators SRRs and cut wire to generate EIT, as illustrated in Fig. 5(a). The bright cut wire and dark SRRs were employed to prompt the electric and magnetic fields. The proposed structure offered a low loss of about 2.5 dB (0.56) at 10.05 GHz with dimensions of 0.7 $\lambda_0 \times$ 0.4 λ_0, as illustrated in Fig. 5(b). The loss was further investigated by surface current distribution. Antiparallel currents were induced on SRRs, leading to a high transmission peak at 10.05 GHz, as shown in Fig. 5(c). In this report, the structure symmetry was maintained, and the distinctive properties of metamaterials

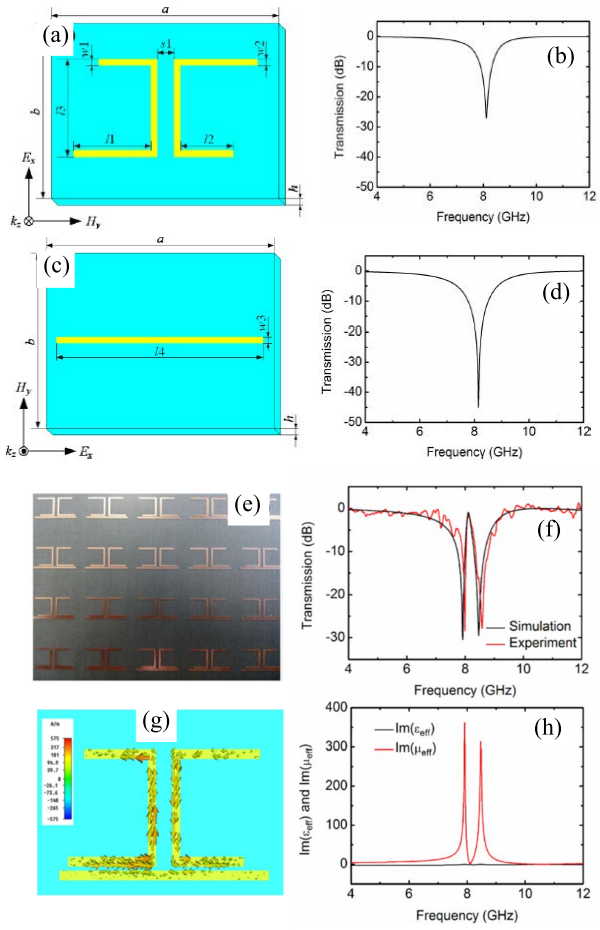

FIGURE 4. EIT-like metamaterial reported in [64]: (a), (b) The schematic view and transmission spectrum of the ASRRs, (c), (d) the schematic view and transmission spectrum of the cut wire shape, (e) the fabricated prototype of the EIT like metamaterial, (f) the simulated and measured transmission spectra, (g) the surface current distribution at 8.12 GHz, and (h) the imaginary parts of ε and μ.

can still be accomplished in the microwave regime. However, the design exhibits a significant loss at the desired frequency. Further, the loss of the conventional SRR was investigated and recompensed based on the EIT phenomenon in [67]. Two SRRs with different dimensions were combined to realize a low-loss system. The metamaterial array with the geometry of the single element and transmission coefficient were displayed in Figs. 6(a) and (b). The strong coupling between the two resonators achieved a transmission peak of 0.5 dB (0.89) at 5.5 GHz. The coupling process was explained by the surface current, in which opposite currents were induced on the wide and narrow SRR leading to a high transmission peak [see Fig. 6(c)]. Nonetheless, the structure loss is significantly high at the microwave spectrum.

Sun *et al.* [68] used SRR to induce the EIT. The structure achieved a transmission peak of 0.55 dB (0.88) at 3.76 GHz. Although the structure exhibits a small physical size of 0.08 $\lambda_0 \times$ 0.08 λ_0, the transmission loss remains high at the low-frequency range. Further, SRRs and I-shape cut wire losses were studied and mitigated using the EIT in [69]

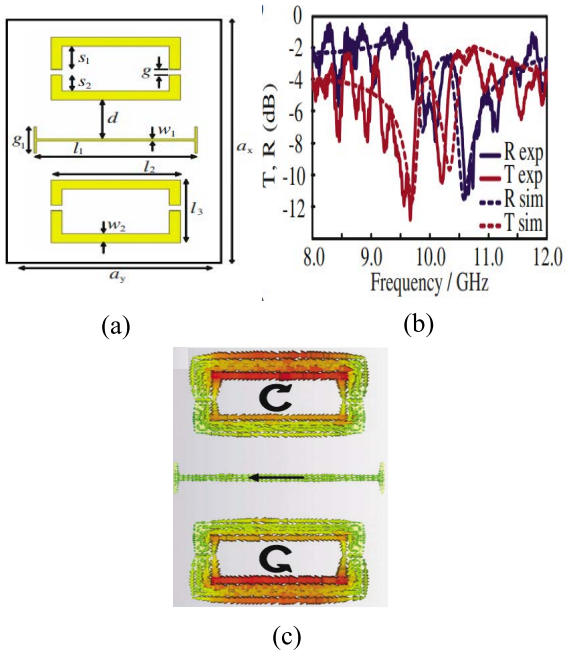

FIGURE 5. EIT-based metamaterial involving SRRs and cut wire [66]: (a) the schematic view of the EIT like metamaterial, (b) the simulated and measured transmission and reflection coefficients, and (c) the surface current distribution at 10.05 GHz.

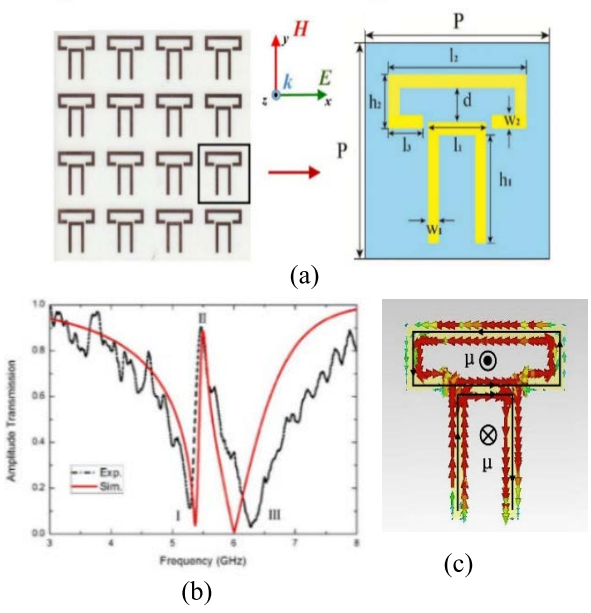

FIGURE 6. EIT-like metamaterial reported in [67]: (a) the array and single unit cell of SRRs, (b) the simulated and measured transmission coefficients, and (c) the surface current distribution at 5.5 GHz.

and [70]. The EIT-like metamaterial in [69] achieved a low loss of 0.97 dB (0.8) at 5.41 GHz. The configuration of dark SRRs and bright I-shape cut wire resonators, and the transmission spectra are illustrated in Figs. 7(a) and (b), respectively. The surface current at the transmission peak was investigated, in which antiparallel currents were observed, as shown in Fig. 7(c). This report provides a low profile

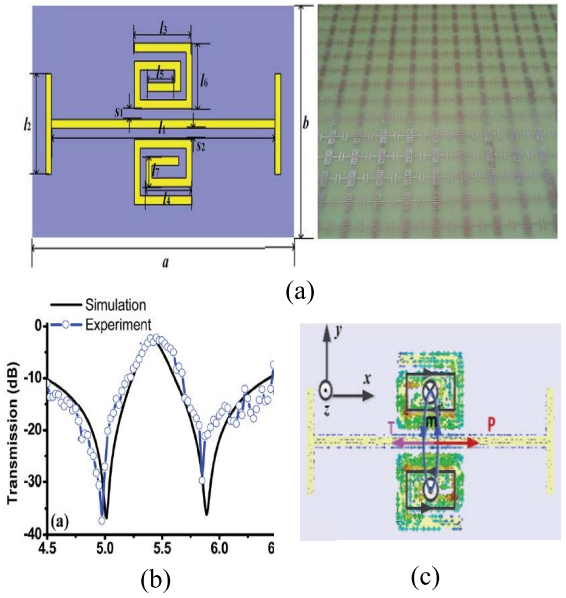

FIGURE 7. EIT based on SRRs and I-shape cut wire [69]: (a) the schematic view and fabricated prototype of EIT like metamaterial, (b) the transmission spectra, and (c) the surface current distribution at 5.41 GHz.

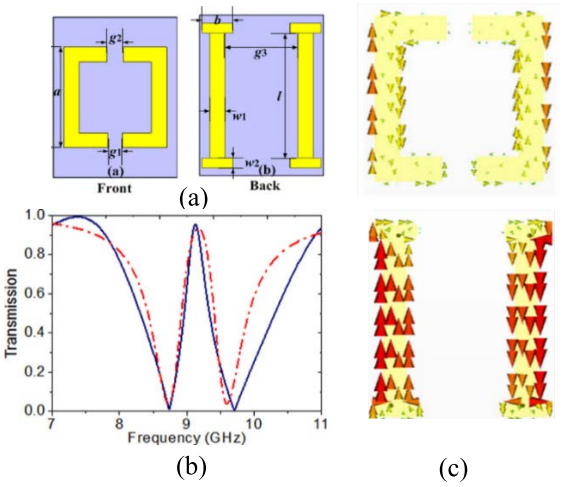

FIGURE 8. EIT-like metamaterial reported in [70]: (a) the configuration of the SRRs and I-shape, and (b) the transmission spectra, and (c) the surface current distribution at 9.1 GHz.

structure with dimensions of 0.3 $\lambda_0 \times 0.2\ \lambda_0$. Zhu *et al.* [70] presented an EIT-like metamaterial with a low loss of 0.26 dB (0.94) at 9.1 GHz. The EIT-like metamaterial was supported by the surface currents of both SRR and cut wire, in which the antiparallel currents were observed in both components leading to destructive interference of the scattering field, thereby inducing a high transmission peak at 9.1 GHz. The metamaterial structure, transmission peak, and the surface current distribution are displayed in Figs. 8(a)-(c), respectively. In [71], Xiang *et al.* studied the loss of asymmetric split-ring resonators (ASRRs) at 13.4 GHz. The structure consists of two split rings printed on the Rogers board, as shown in Fig. 9(a). A high transmission peak of 0.41 dB

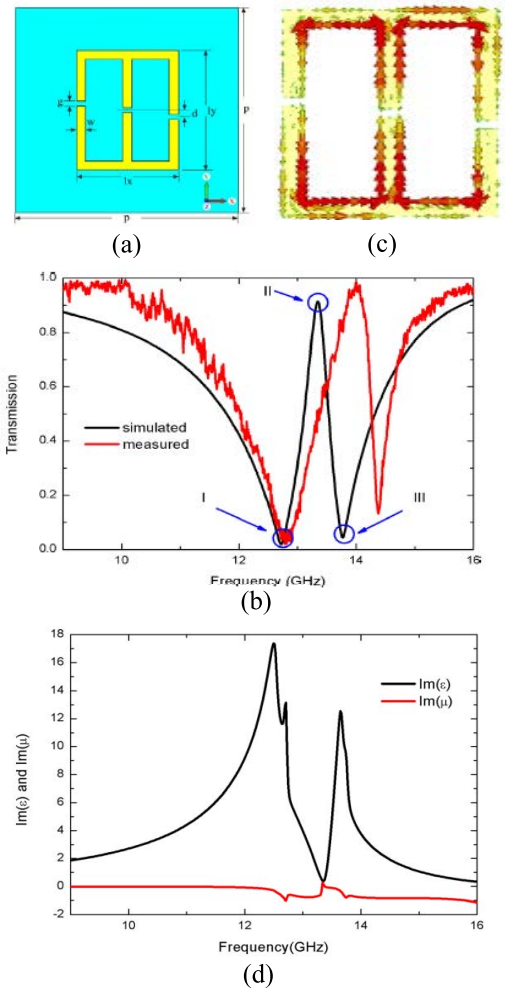

FIGURE 9. The loss suppression approach reported in [71]: (a) the fabricated sample of the ASRRs and the single unit cell structure, (b) the simulated and measured transmission spectra, (c) the surface current at 13.4 GHz, and (d) the imaginary values of ε and μ.

(0.91) was obtained at 13.4 GHz, as illustrated in Fig. 9(b). The structure induces opposite currents in the two split rings, which helps explain the loss suppression mechanism, cf. 9(c). Moreover, the imaginary parts of ε and μ were calculated at the resonant frequency based on the effective medium theory and plotted in Fig. 9(d), in which their values were approaching zero at 13.4 GHz. The double-split ring resonator (DSRR) and square ring resonator (SqRR) were combined by Bagci and Akaoglu [72] to realize EIT-like metamaterial. The transmission peak of 0.96 dB (0.8) was obtained at 0.87 GHz. Zhu *et al.* [73] proposed a new metamaterial to realize EIT. Two cylindrical through-hole cubes (CTCs) induced the EIT-like metamaterial at the microwave regime. Two different dimensions of CTCs offered electric and magnetic resonances in the proximity of 6.2 GHz. The destructive interference of scattering fields can be obtained by adjusting the interaction between these CTCs, thereby inducing EIT and suppressing the loss. High transmission of 0.45 dB (0.9) was achieved at 6.2 GHz.

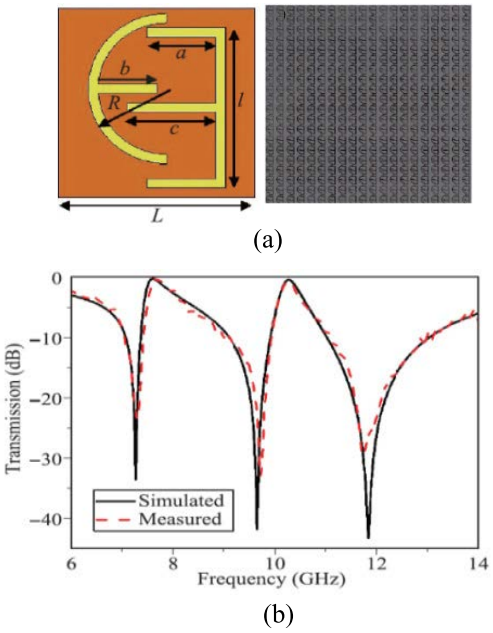

FIGURE 10. The E-ε EIT metamaterial reported in [75]: (a) single unit cell configuration and the fabricated periodic structure, and (b) the simulated and measured transmission spectra.

Miniaturization and cost-effectiveness are usually required to design high performance devices. These merits can be obtained by developing multi-band metamaterial-based devices. Different dual-band designs have been proposed in the literature for various applications [76]–[78]. The EIT metamaterials with dual-band and low loss properties at microwave regime were reported in [74] and [75]. In [74], Zhu *et al.* proposed three ceramic blocks with different dimensions to obtain the EIT-like metamaterial. The transmission windows were observed at 6.24 and 6.38 GHz with peaks of 2.2 dB (0.6) and 4.3 dB (0.37), respectively. Shen *et al.* [75] combined the E-and the ε-shapes in one unit cell to build a dual-band EIT metamaterial. The E-ε structure provided low loss with transmission peaks of 0.31 dB (0.93) and 0.49 dB (0.89) at 7.60 GHz and 10.27 GHz, respectively. The configuration of the E-ε EIT metamaterial and the fabricated prototype are depicted in Fig. 10(a), while the simulated and measured transmission spectra are displayed in Fig. 10(b). The millimeter-wave spectrum is being used for many modern applications. Many metamaterial structures were designed at this band for achieving different functionalities, such as high absorbance and super-lens [79], [80]. It is known that the increase of the operating frequency to high range such as millimeter-wave is associated with high loss, which should be mitigated to boost the performance of the devices at this band. Few works were focused on studying the metamaterial losses at the millimeter-wave spectrum due to fabrication and measurement limitations [81]–[83]. Further, most of the devices based on metamaterial work at the microwave spectrum. Esmail *et al.* [81] proposed a modified double square ring resonator (MDSRR) for obtaining a very low loss of 0.5 dB (0.89) at 76 GHz. The principle of the

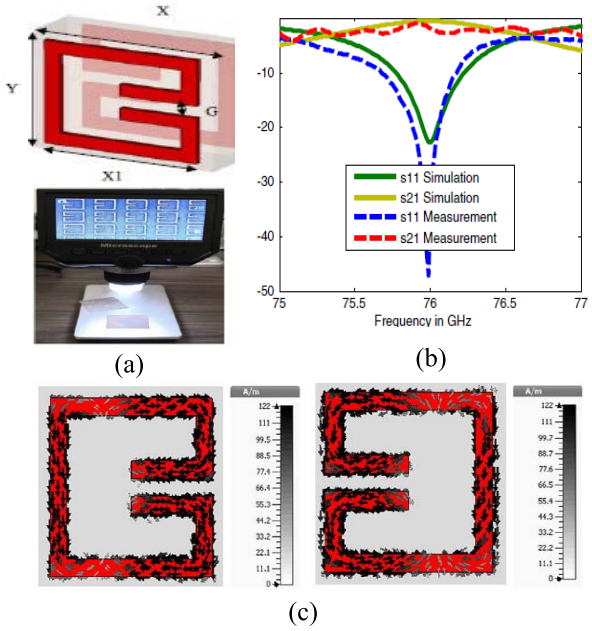

FIGURE 11. The EIT based on MDSRR [81]: (a) schematic view of the MDSRR and the fabricated prototype, (b) the simulated and measured transmission and reflection spectra, and (c) the surface current on both sides of the unit cell at 76 GHz.

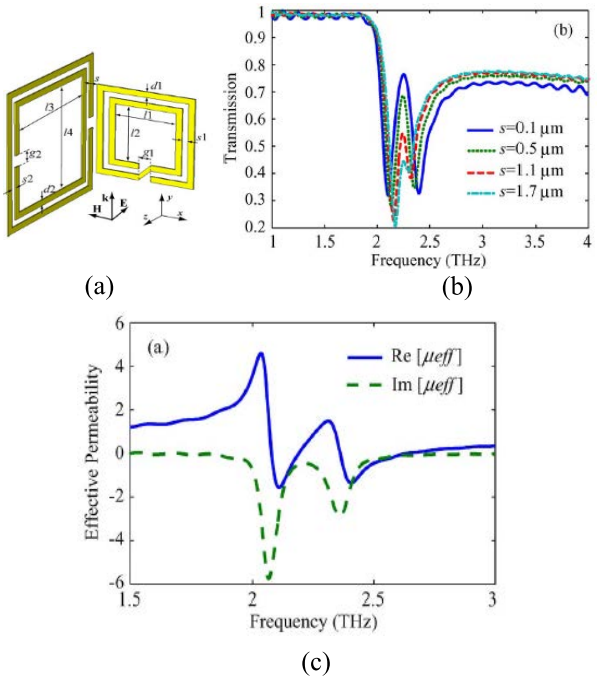

FIGURE 12. EIT metamaterial reported in [86]: (a) configuration of the SRR and SR structures, (b) the transmission window at 2.25 THz, and (c) the real and imaginary of μ.

EIT based on the antiparallel surface currents was used to explain the low loss mechanism. The designed configuration and the fabricated prototype are displayed in Fig. 11(a), while simulated and measured S-parameters are presented in Fig. 11(b). The surface currents of both sides at 76 GHz are illustrated in Fig. 11(c). The losses of the MDSRR, S-shape, G-shape, and Ω-shape were studied and compared at 28 GHz, in which the MDSRR provided the lowest loss compared to other structures [83].

As mentioned earlier, the metamaterials exhibit high loss when the frequency increases to a higher range. Therefore, many reports proposed methods for compensating their inherent loss at the terahertz spectrum [58], [84]–[90]. The reduced number of published works and the loss investigation in the simulation stage only are due to fabrication challenges at this band. The loss of the conventional metamaterials based on EIT at 0.5 THz was discussed in [84]. The double-gap split ring resonator (DSRR) induced dark mode, whereas a straight metallic strip stimulated the bright mode. The coupling between the two resonators was optimized to reduce the inherent loss. This report achieved a loss of 3 dB (0.5) at 0.5 THz with a physical size of 0.4 $\lambda_0 \times$ 0.4 λ_0. Tassin *et al.* [85] proposed an EIT based on double split-ring resonators to provide a low loss and high absorption at 42.5 THz. One ring was responsible for inducing dark mode, and the other caused the radiative mode. The coupling between the two rings can be controlled by adjusting their distance. The proposed structure achieved a transmission peak of about 0.09 dB (0.98) at 42.5 THz. Moreover, the imaginary part of μ approximated zero, indicating low loss at the transparency window. Further, Meng *et al.* [86] proposed SRR and a spiral resonator (SR) to operate as radiative and dark resonances. Figure 12(a) depicts the configuration of the two structures. The coupling depended on the separation between the SRR and SR, which led to the transmission window with a peak of 1.13 dB (0.77) at 2.25 THz, as presented in Fig. 12(b). The low loss property was confirmed by the small imaginary value of the μ as shown in Fig. 12(c). Moreover, the conventional SRR was used in [58] to induce EIT-like metamaterial at 77 THz. In this report, the outer ring with two gaps was chosen to excite the radiative modes, whereas the inner ring excited a dark mode. The transmission window appeared at 77 THz with a peak of 0.09 dB (0.98). The configuration of the SSR and the transmission spectra of the outer, inner, and double rings are shown in Figs. 13(a) and (b). The low imaginary of the ε and μ supported a low loss property at the transmission window, as illustrated in Fig. 13(c). The dual-band low-loss EIT-like metamaterial at THz was reported by Liu *et al.* in [88]. The structure is composed of the cut wire (bright resonator) placed between the double-split rings (dark resonator). The consolidation between the two resonators exhibited dual transmission windows with peaks of 0.04 dB (0.99) at 0.39 THz and 0.26 dB (0.94) at 0.55 THz. In [89], the authors proposed an EIT-like metamaterial consisting of a metal strip that served as the radiative mode and two parallel metal strips that worked as the dark mode. The spatial separation of the two components determines the coupling between the two modes, in which the strong coupling induced a high transmission peak at 428.4 THz. Gu *et al.* [90] employed a cut wire and SRR to exhibit EIT at 0.74 THz.

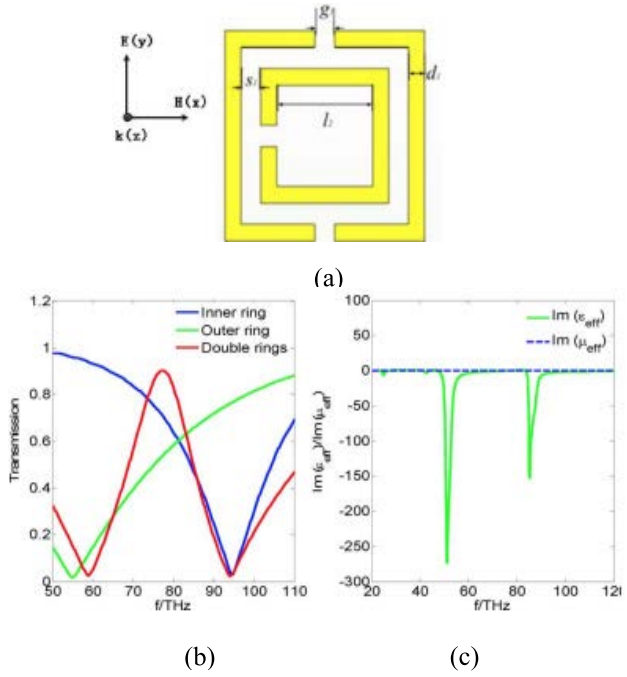

FIGURE 13. The loss compensation reported in [58]: (a) the conventional SRR, (b) the transmission spectra of the outer, inner and SRR, and (c) the imaginary part of the ε and μ.

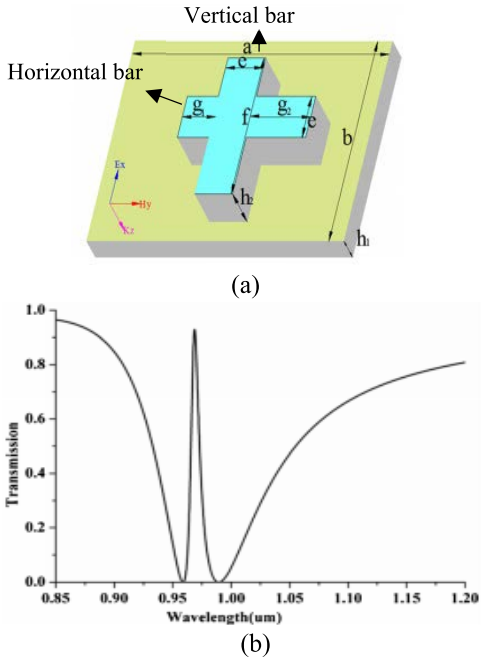

FIGURE 14. EIT like metamaterial based of [95]: (a) the metamaterial with horizontal and vertical bar structures, and (b) the simulated transmission.

The cut wire resulted in a localized surface plasmon (LSP) resonance. On the other hand, the coupling between the cut wire and the SRRs excited the inductive–capacitive (LC) resonance. A sharp transparency peak at 0.74 THz was obtained due to destructive interference between the LSP and LC resonances.

The low loss-based EIT-like metamaterial at telecommunication wavelength was investigated in [91]–[95]. In [91], the SRR and paired nano-rods were used to obtain bright and dark modes. The strong coupling between the two modes induced a transmission peak of approximately 0.45 dB (0.9) at 1560 nm. Qin *et al.*. presented a U-shaped metamaterial made of silicon on a quartz substrate for achieving a low loss of 0.36 dB (0.92) at 908.5 nm [92]. To support the low loss property, the structure introduced FOM of 29 and Q-factor of 130. The analogy of EIT behavior can be obtained by an array of silicon rods on the quartz waveguide layer [94]. The structure was optimized by adjusting the separation of unit cells and the thickness of the waveguide layer for achieving destructive interference between the magnetic resonant and guide mode resonance, in which a transmission window with a high peak of 0.26 dB (0.94) was obtained at 604 nm. The structure exhibits a very high Q factor of 10000. In [95], Wei *et al.*. presented two mutually perpendicular silicon bars to study the loss based on EIT at the telecommunication wavelength [see Fig. 14(a)]. The vertical and horizontal bars were chosen as the radiative and the dark modes. The strong coupling was obtained by changing the length of the two bars, thereby obtaining a high transmission peak of 0.32 dB (0.93) at 968 nm, as illustrated in Fig. 14(b). Further, a high FOM of 42 and a Q-factor of 139 were obtained to support the low loss property.

Although this method ensures low losses, which are close to zero, it has a serious drawback: the long time required for coupling between metamaterial unit cell components for inducing the bright and the dark modes. Further, some designs lose the negativity in the real part of constitutive parameters, and provide a narrow bandwidth of low loss. The summary of metamaterial loss reduction based on EIT is presented in Table 1.

B. LOSS MITIGATION BASED ON GEOMETRIC TAILORING OF THE METAMATERIALS

The losses will restrict the application range of metamaterials and delay their incorporation into functional devices except if effective ways of loss reduction are developed. As mentioned earlier, the EIT-like metamaterial is the most popular approach for obtaining a low loss metamaterial. However, another approach based on geometric tailoring of the structure was also proposed in the literature for loss mitigation [62]. The geometric tailoring approach is implemented by optimizing the parameters of the structure to provide a low loss behavior [56], [57], [59], [60], [96]–[116].

Different shapes of SRRs were studied to reduce the ohmic loss at low and high frequencies [56]. One of the major contributors to the ohmic losses are conducting layers. Another might be geometrical features, which may exhibit significant loss due to field concentration and non-uniform current distribution. The loss can be reduced by redistributing the surface current using different SRR shapes. In addition,

TABLE 1. Summary of metamaterial loss reduction based on EIT approach.

Ref.	Metamaterial shape (physical size)	Frequency regime (frequency/wavelength)	Transmission loss (linear scale)	Additional measures of the loss
[64]	ASRR and cut wire ($0.43\ \lambda_0 \times 0.43\ \lambda_0$)	Microwave regime (8.12 GHz)	0.56 dB (0.88)	Low imaginary values of μ and ε
[66]	SRRs and cut wire ($0.7\ \lambda_0 \times 0.4\ \lambda_0$	Microwave regime (10.05 GHz)	2.5 dB (0.56)	The surface current was used to explain the loss reduction mechanism
[67]	SRR ($0.3\ \lambda_0 \times 0.3\ \lambda_0$)	Microwave regime (5.5 GHz)	0.5 dB (0.89)	The imaginary values of μ and ε were approximately zero
[68]	SRR ($0.08\ \lambda_0 \times 0.08\ \lambda_0$)	Microwave regime (3.76 GHz)	0.55 dB (0.88)	—
[69]	SRRs and I-shape cut wire ($0.3\ \lambda_0 \times 0.2\ \lambda_0$)	Microwave regime (5.41 GHz)	0.97 dB (0.8)	The imaginary value of the refractive index was approached zero
[70]	SRRs and I-shape cut wire ($0.3\ \lambda_0 \times 0.2\ \lambda_0$)	Microwave regime (9.1 GHz)	0.26 dB (0.94)	The surface current was used to explain the loss reduction mechanism
[71]	ASRRs ($0.53\ \lambda_0 \times 0.53\ \lambda_0$)	Microwave regime (13.4 GHz	0.41 dB (0.91)	The surface current and the low imaginary values of μ and ε
[72]	DSRR and SqRR ($0.35\ \lambda_0 \times 0.07\ \lambda_0$)	Microwave regime (0.87 GHz)	0.96 dB (0.8)	The surface current was used to explain the loss reduction mechanism
[73]	Two CTCs Large CTC ($0.13\ \lambda_0 \times 0.13\ \lambda_0$) Small CTC ($0.1\ \lambda_0 \times 0.1\ \lambda_0$)	Microwave regime (6.2 GHz)	0.45 dB (0.9)	High Q-factor
[74]	Three ceramic blocks ($0.33\ \lambda_0 \times 0.33\ \lambda_0$) at the lower band	Microwave regime (6.24 and 6.38 GHz)	2.2 dB (0.6) at 6.24 GHz and 4.3 dB (0.37) at 6.38 GHz	—
[75]	E-ε structure ($0.25\ \lambda_0 \times 0.25\ \lambda_0$) at the lower band	Microwave regime (7.60 GHz and 10.27 GHz)	0.31dB (0.93) at 7.60 GHz and 0.49 dB (0.89) at 10.27 GHz	High Q-factor at both frequencies
[81]	MDSRR ($0.25\ \lambda_0 \times 0.22\ \lambda_0$)	Millimeter-wave regime (76 GHz)	0.5 dB (0.89)	The surface current was used to explain the loss reduction mechanism
[83]	MSRR ($0.25\ \lambda_0 \times 0.22\ \lambda_0$)	Millimeter-wave regime (28 GHz)	0.1 dB (0.97)	The surface current was used to explain the loss mechanism
[84]	DSRR and the straight metallic strip ($0.4\ \lambda_0 \times 0.4\ \lambda_0$)	Terahertz regime (0.5 THz)	3 dB (0.5)	—
[85]	Double SRRs ($0.12\ \lambda_0 \times 0.12\ \lambda_0$)	Terahertz regime (42.5 THz)	0.09 dB (0.98)	The low imaginary value of μ
[86]	SRR ($0.11\ \lambda_0 \times 0.11\ \lambda_0$) and SR ($0.06\ \lambda_0 \times 0.06\ \lambda_0$)	Terahertz regime (2.25 THz)	1.13 dB (0.77)	A minimal imaginary value of the μ
[58]	SSR ($0.27\ \lambda_0 \times 0.27\ \lambda_0$)	Terahertz regime (77 THz)	0.09 dB (0.98)	The imaginary values of μ and ε were minimal
[88]	DSRR and cut wire ($0.26\ \lambda_0 \times 0.15\ \lambda_0$) at lower band	Terahertz regime (0.39 THz and 0.55 THz)	0.04 dB (0.99) at 0.39 THz and 0.26 dB (0.94) at 0.55 THz	—
[91]	SRR and paired nano-rods ($0.51\ \lambda_0 \times 0.51\ \lambda_0$)	Telecommunication wavelength (1560 nm)	0.45 dB (0.9)	—
[92]	Vertical and horizontal rods unit cell ($0.68\ \lambda_0 \times 0.68\ \lambda_0$)	Telecommunication wavelength (908.5 nm)	0.36 dB (0.92)	High values of FOM and Q-factor
[94]	Silicon rods ($0.66\ \lambda_0 \times 0.72\ \lambda_0$)	Telecommunication wavelength (604 nm)	0.26 dB (0.94)	The structure afforded a high Q factor
[95]	Two mutually perpendicular silicon bars ($0.78\ \lambda_0 \times 0.76\ \lambda_0$)	Terahertz regime (310 THz)	0.32 dB (0.93)	High value of FOM

reducing the skin depth and removing the sharp edges can be considered solutions for mitigating the loss at a high-frequency range. Zhou *et al.* [97] studied the loss based on the double bowknot-shaped structure (DBS) at 11 GHz. The interference between the electric and magnetic resonances was exploited to realize a low loss structure. By tailoring the geometrical properties of DBS, three types (A, B, and C) with low losses were obtained. The types A, B, and C offered losses of 2.75 dB (0.53), 2.3 dB (0.59), and 1.33 dB (0.74) at 11 GHz, respectively. The structure parameters, L and C, can be exploited to alleviate the loss [57], [98]–[101]. As it is known, the losses of the RLC circuit rely on circuit parameters and the Q-factor. The decline in the capacitance, C, and resistance, R, or the increment in the inductance, L, causes a rise in the Q-factor, thereby alleviating the circuit loss. The fishnet structure and a circular spiral split ring resonator (CSSRR) were proposed by Zhou *et al.* [57] and Shaw and Mitra [98], respectively, to achieve low loss structures. The structure parameters of both designs were optimized through EM simulations to raise the L/C ratio, thereby raising the Q-factor and mitigating the loss. In [99], the authors proposed the adjacent square-shaped resonator (ASSR) with low loss at 3.5 GHz. The equivalent circuit was presented to validate the simulation results and explain the low loss property. The ASSR achieved a low loss of 0.2 dB (0.95) at 3.5 GHz. The single and dual-band low loss at the high-frequency range were studied in [100] and [101], respectively. Chiral Metamaterials (CMM) is an alternative way for achieving a negative refractive index. In such materials, the chirality parameter, κ, is used to quantify the coupling between the electric and magnetic fields needlessly to induce simultaneously negative μ and ε. Fernandez *et al.* [102] combined the conjugated gammadion (CG) structure and fishnet structure to form a fishnet chiral metamaterial (FCMM) structure with low loss. The FCMM was optimized by including a metallic patch that counterbalances the inductive response of the fishnet wires. The FCMM minimized the loss to 0.91 (0.81) at 10.8 GHz and maximized the bandwidth up to 0.77 GHz with maintaining a negative refractive index. Further, the structure achieved a FOM of 38. Sun *et al.* [103] optimized the distance between the neighbouring SRRs to build negative-index metamaterial with low loss property at the microwave spectrum. The short distance introduced a strong coupling effect, contributing to low loss property. The loss was verified by the near-zero imaginary part of μ at 9 GHz. In [104], the ferrimagnet with minor loss was utilized to replace the SRRs for attaining a negative μ, while the printed circuit boards (PCBs) achieved a negative ε. A low loss with a transmission peak of 2.5 dB was obtained by controlling the applied magnetic field at 10 GHz. The zero index metamaterials (ZIMs) can be obtained when either ε or μ (or both) are zero, where this class of metamaterials is utilized in broad range of applications. The low loss-based ZIMs was reported in [105] and [106]. Ma *et al.* [105] proposed ZIM-based wires on the surface and through the substrate. By adjusting the electric and magnetic

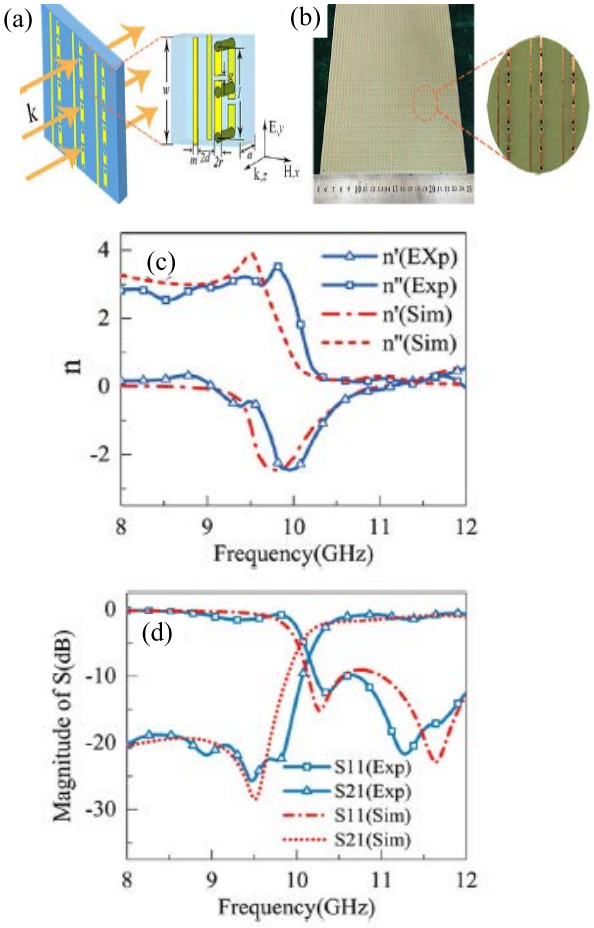

FIGURE 15. Low loss ZIMs proposed in [105]: (a) the schematic view of the periodic ZIM metamaterial, (b) the fabricated photograph of the ZIM array, (c) the refractive index, and (d) the simulated and measured transmission and reflection spectra.

plasma frequencies, a low loss of 1.7 dB was obtained in the range of 10.72–11.4 GHz. Figures 15(a) and (b) show the designed and fabricated ZIM, respectively. The refractive index and the transmission spectra with broad low loss property are illustrated in Figs. 15(c) and (d). Moitra *et al.* proposed all-dielectric ZIM with a very low loss in the range of 1432–1457 nm [106]. The loss mitigation based on geometric tailoring at the millimeter-wave regime was discussed in [107]–[109]. The center symmetric "T" shaped unit cell with wide bandwidth and low loss was proposed by He *et al.* [107]. The configuration and the photography of the fabricated structure are depicted in Fig. 16(a). Due to the proper geometrical arrangement of four symmetric "T" metallic shapes on the front side of the substrate layer, a broad negative refractive index in the range of 20.16–37.47 GHz with relative width of 60.07%, a low loss of 0.32 dB, and miniature size of 0.07 λ_0 × 0.07 λ_0 were achieved. Figures 16(b) and (c) display the broad negative reflective index and transmission and reflection spectra. The losses of the double E-shaped resonator (DER) and T-U shaped resonator (TUSR) were studied and reduced

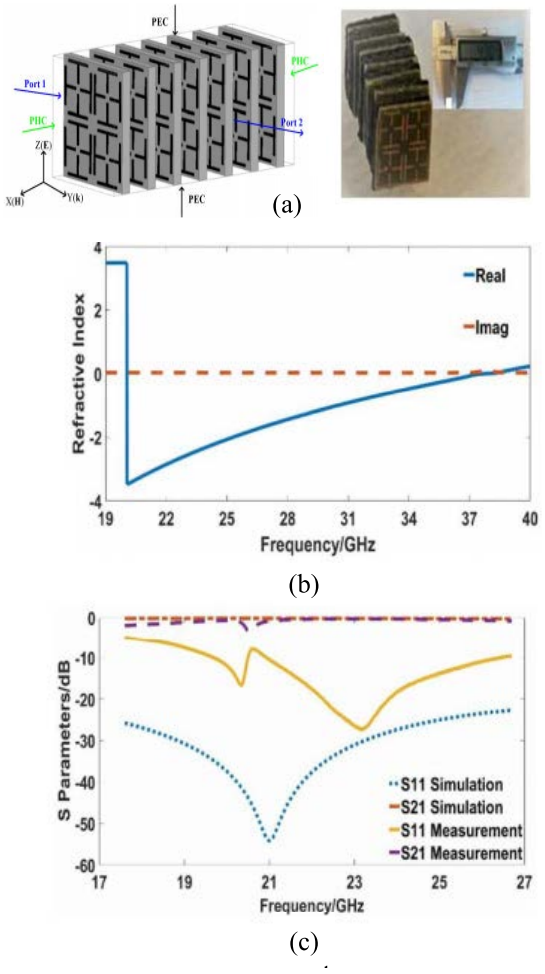

FIGURE 16. The broad low loss metamaterial proposed in [107]: (a) the configuration and fabricated prototype of the center symmetric "T" metamaterial, (b) the refractive index, and (c) the simulated and measured transmission and reflection spectra.

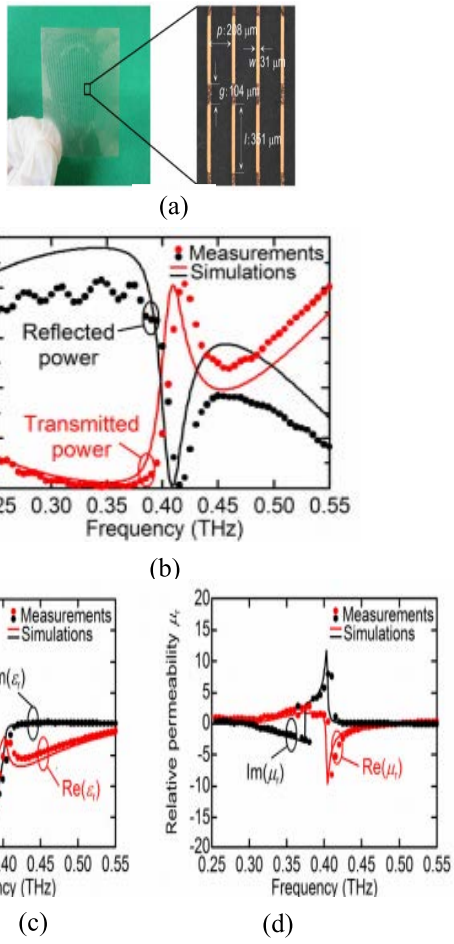

FIGURE 17. Low loss cut wire structure based of [110]: (a) the fabricated photograph; inset, magnified view, (b) the transmitted and reflected power, the real and imaginary parts of the (c) ε and (d) μ.

at 28 GHz [108]. Due to the proper geometrical arrangement, the losses were reduced to 0.09 dB and 0.23 dB for DER and TUSR, respectively. Alici and Ozbay designed the composite metamaterial medium (CMM) for providing a low loss of 2.5 dB at 100 GHz [109]. The losses mitigation is crucial, especially at a high-frequency range like the terahertz spectrum. Consequently, the researchers proposed different structures with advanced fabrication methods to alleviate such losses at this band [110]–[113]. The asymmetrically aligned paired cut wires on both sides of the cyclo-olefin polymer substrate were proposed by Suzuki *et al.* [110] to provide low loss at 0.42 THz. The transmitted power of 81.5% was achieved by breaking structure symmetry. The fabricated photograph of the periodic structure and the transmitted power are illustrated in Figs. 17(a) and (b). The ε and μ were also studied to support the low loss property, in which the imaginary parts of both were approaching zero at 0.42 THz [see Figs. 17(c) and (d)]. Askari *et al.* [111] presented a semi H-shaped resonator (SHR) with low loss at 4.725 THz. The proper geometrical arrangement of the structure offered a low loss of 0.65 dB (0.86) and a low reflection of −16.48 dB at 4.725 THz. The split range resonator, bar shapes, and bow-tie were printed on parylene film and silicon substrates to build a flexible and low loss metamaterial, as shown in Figs. 18(a), (b), and (c) [112]. It is founded that the three metamaterial structures provided low loss and high Q-factor when they were printed on the silicon wafer, as illustrated in Figs. 18(d), (e), and (f), while the loss was further mitigated when structures were fabricated on the parylene film, as depicted in Figs. 18(g) and (h). The gaps of the three structures played an essential role in optimizing the loss and providing a high Q-factor. This work presented flexible and low-loss structures, which were proposed for biosensing applications. The fishnet structure is one of the more extensively explored metamaterial structures at telecommunication wavelengths. Its loss was studied in many reports [59], [60], [114]–[116]. Due to the silver's lower damping, it was printed on the glass substrate to build a low loss negative-index metamaterial at the telecommunication wavelengths [60]. The measured transmittance and the FOM have reached 0.75 and 3 at 1.4 μm, respectively. Iyer *et al.* [114] optimized the hole shape of the fishnet

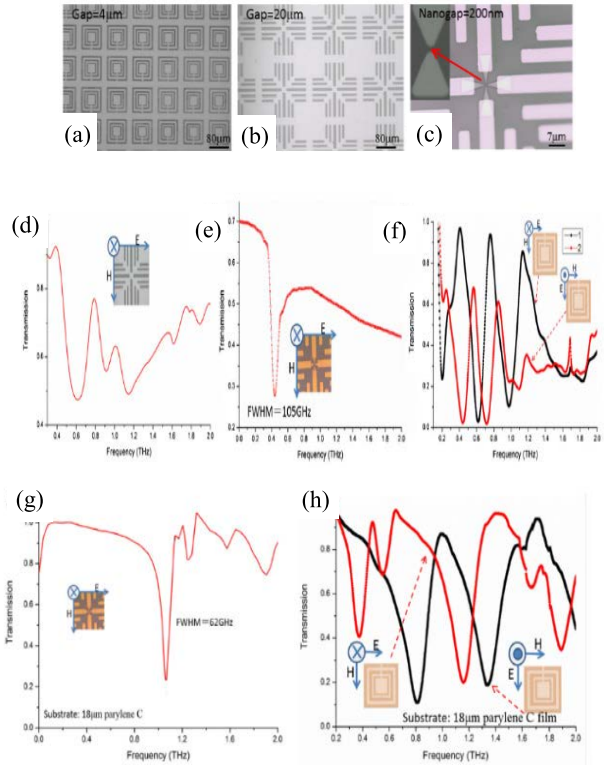

FIGURE 18. Low loss terahertz metamaterials proposed in [112]: (a) three split rings, (b) bar shape and (c) bow-tie. The transmission spectra of the three metamaterial shapes on silicon substrate (d) bar shape, (e) bow-tie and (f) three split rings. The transmission spectra of the metamaterial shapes on parylene C film substrate (g) bar shape and (h) three split rings.

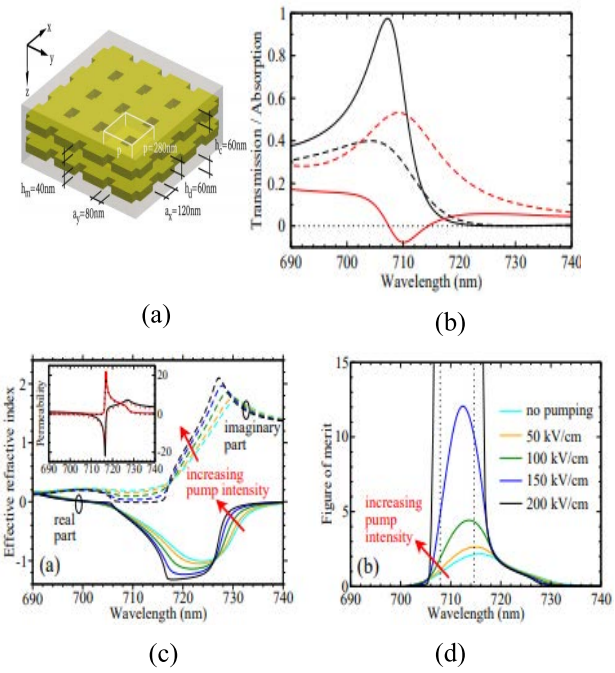

FIGURE 19. The gain material for loss compensation proposed in [121]: (a) the silver double-fishnet structure and dye molecules in the dielectric host material, (b) the transmission (black) and absorption (red) with (solid lines) and without gain material (dashed lines), (c) the refractive index, and (d) FOM at different electric field amplitudes.

within 1.4–1.5 μm, in which the elliptical holes provided lower loss than the rectangular ones, resulting in a FOM of roughly 6. Further, Yun *et al.* [115] optimized the electric and magnetic responses of the fishnet structure by adjusting the metallodielectric nanostructures to obtain low loss property at a wavelength of 1.55 μm. The hybrid metal-semiconductor nanowires were proposed by Paniagua-Domınguez *et al.* to achieve a low loss property at 1.4 μm [116]. By optimizing these nanowires, the transmittance and the FOM reached a high of 0.97 and 200, respectively. The main advantages of this approach are the acceptable low loss, the low fabrication cost, and the broad bandwidth of low loss provided by some designs. Nevertheless, this technique is based on human intuition and lacks systematic procedures for obtaining low loss. Furthermore, it is a time-consuming approach compared to other (systematic) methods. The summary of the low loss metamaterials based on the geometric tailoring method is presented in Table 2.

C. EMBEDDING THE GAIN MATERIALS FOR LOSS COMPENSATION

Another promising approach to loss compensation is by including gain materials. This is a promising approach, in which zero-loss metamaterials can be predicted theoretically, even over a wide bandwidth. Nevertheless, it may not always be possible to find proper material to ensure the required gain at the desired frequency band [33]. It is common to assume that the metamaterials and the gain materials are independent [117], [118]. Incorporating such materials changes the metamaterial properties, thereby altering the coupling to the gain material until reaching a steady state. The loss compensation relies on the strong coupling between the meta-atoms of the metamaterials and the gain material [119]. Several gain materials can be incorporated into the metamaterial structures for loss compensation, including organic dye molecules, semiconductors, quantum dots, and quantum wells [120]–[126]. The fishnet structure with a gain medium was studied numerically and experimentally by Xiao *et al.*. to overcome the loss at visible wavelengths [120]. Therein, the epoxy with dye molecules was used as a gain material. The loss was studied in terms of transmission, FOM, and the constitutive parameters. The FOM reached a height of 26, and the imaginary constitutive parameters, ε, μ, and refractive index, approached zero at 738 nm. Further, Wuestner *et al.*. [121] used dye molecules as the gain material for mitigating losses of the double fishnet structure at 710 nm. The structure loss was investigated theoretically and numerically. The fishnet structure with dye molecules incorporated in the dielectric layer is depicted in Fig. 19(a). The transmission, effective refractive index, and FOM were studied to explain the low loss property, as shown in Figs. 19(b), (c), and (d). Bratkovsky *et al.*. [124] combined silver rods with quantum dots (QDs) for compensating the

TABLE 2. Summary of the low loss metamaterials based on the geometric tailoring approach.

Ref.	Metamaterial shape (physical size)	Frequency band	Transmission peak (linear scale)	Additional measures of the loss
[96]	Bridge-shaped resonator (BSR) ($0.34\,\lambda_0 \times 0.34\,\lambda_0$)	Millimetre-wave regime 28 GHz	0.06 dB (0.98)	—
[97]	DBS ($0.3\,\lambda_0 \times 2.7\,\lambda_0$)	Microwave regime 11 GHz.	-Type A= 2.75 dB (0.53), -Type B= 2.3 dB (0.59) -Type C= 1.33 dB (0.74)	High value of FOM
[98]	CSSRR ($0.23\,\lambda_0 \times 0.23\,\lambda_0$) at lower band 8.82 GHz	Microwave regime 8.82 GHz 13.93 GHz, and 18.02 GHz	—	High value of FOM and low imaginary values of ε and μ
[99]	ASSR ($0.1\,\lambda_0 \times 0.1\,\lambda_0$)	Microwave regime 3.5 GHz	0.2 dB (0.95)	Low imaginary value of the refractive index
[100]	SRR ($0.22\,\lambda_0 \times 0.22\,\lambda_0$)	Millimetre-wave regime 27.5 GHz	0.17 dB (0.96)	—
[101]	MSSR ($0.2\,\lambda_0 \times 0.2\,\lambda_0$)	Millimetre-wave regime 28 GHz and 32.54 GHz	0.3 dB (0.93) at 28 GHz and 0.18 dB (0.95) at 32.54 GHz	—
[102]	FCMM ($0.36\,\lambda_0 \times 0.36\,\lambda_0$)	Microwave regime 10.8 GHz	0.91 (0.81)	High value of FOM
[103]	SRRs ($0.3\,\lambda_0 \times 0.15\,\lambda_0$)	Microwave regime 9 GHz	—	The imaginary part of μ approached zero
[104]	The ferrimagnet with minor loss was utilized to replace the SRRs for attaining a negative μ, while the printed circuit boards (PCBs) achieved a negative ε	Microwave regime 10 GHz	2.5 dB (0.56)	—
[105]	S-shaped with wires ($0.18\,\lambda_0 \times 0.11\,\lambda_0$)	Microwave regime 10.72-11.4 GHz	1.7 dB (0.67)	—
[107]	Symmetric "T" metallic shape ($0.15\,\lambda_0 \times 0.15\,\lambda_0$)	Millimetre-wave regime 21.12 GHz and 35.10 GHz	0.32 dB (0.92)	The imaginary value of the refractive index approached zero
[108]	DER and TUSR ($0.31\,\lambda_0 \times 0.32\,\lambda_0$)	Millimetre-wave regime 28 GHz	0.09 dB (0.97) for DER and 0.23 dB (0.94) for TUSR	—
[109]	CMM ($0.37\,\lambda_0 \times 0.18\,\lambda_0$)	Millimetre-wave regime 100 GHz	2.5 dB (0.56)	Low imaginary value of the refractive index
[110]	Cut wires ($0.5\,\lambda_0 \times 0.4\,\lambda_0$)	Terahertz regime 0.42 THz	0.91 dB (0.81)	High value of FOM
[111]	SHR ($1\,\lambda_0 \times 0.08\,\lambda_0$)	Terahertz regime 4.7 THz	0.65 dB (0.86)	High value of FOM and low imaginary value of the refractive index

metallic loss. The spherical Indium arsenide (InAs)/Gallium arsenide (GaAs) QDs were employed as an optical pump to provide the required gain. This structure exhibited a negative ε with a low loss at 1.55 μm. The imaginary of ε was approached zero (≈ -0.02), which indicates a low loss property. Further, in [125], lead sulfide (PbS) QDs gain media was included in the fishnet structure to provide low metallic loss at telecommunication wavelength, as illustrated in Fig. 20(a). By embedding the gain material, the transmission peak was approaching 0 dB at 1.5 μm [see Fig. 20(b)]. For demonstrating the low loss property further, the constitutive parameters, ε and μ, were studied at the desired band [see Figs. 20(c) and (d)]. Furthermore, Meinzer *et al.*. used the gain material to overcome the loss of SRR array at telecommunication wavelength [126]. The InGaAs single quantum well was coupled with the silver SRR structure to compensate the metallic loss at 1.5 μm. Fang *et al.*. [127] presented the silver-based SRR with a gain layer underneath for loss mitigation at the terahertz spectrum. The structure was designed on a GaAs-gain-GaAs sandwich substrate. In [128] and [129], the gain material was incorporated into the gap of SRR to compensate the loss, as depicted in Fig. 21(a). The μ and the refractive index of the SRR with and without the gain material were retrieved at the terahertz spectrum, as illustrated in Figs. 21(b) and (c). The influence of the metamaterial loss on the superresolution devices was studied in [130]–[132]. The conventional SRR and wire structure were utilized as the building block of the low loss metamaterial. Lagarkov *et al.* [131], [132] compensated the metamaterial loss by using the active medium at the optical spectrum. The authors in [133] and [134] used the active gain medium to reduce the loss

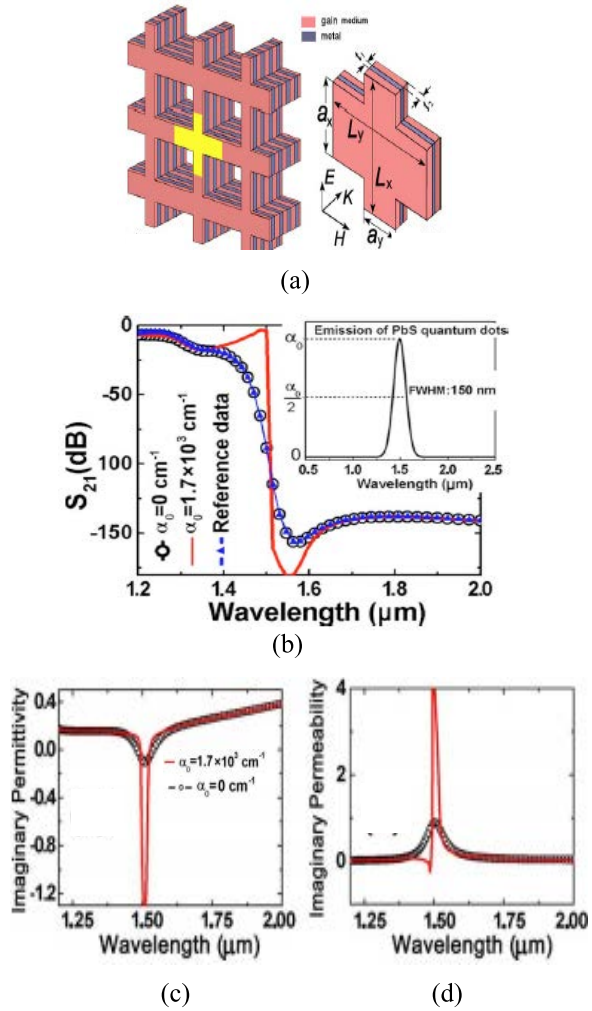

FIGURE 20. The QDs gain material for loss compensation proposed in [125]: (a) schematic view of the fishnet structure with four metallic layers and PbS QDs gain material, (b) transmission spectra of the ten-layer fishnet metamaterial without gain ($\alpha_0 = 0\ cm^{-1}$) and with gain ($\alpha_0 = 1.7 \times 10^3\ cm^{-1}$), and imaginary constitutive parameters (c) ε, (d) μ.

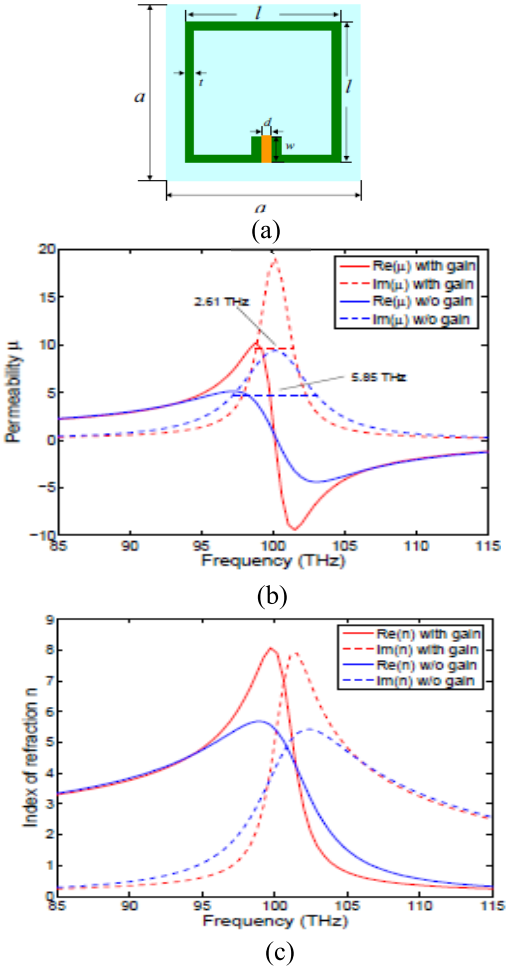

FIGURE 21. SRR incorporated gain material for loss compensation proposed in [128]: (a) schematic view of the SRR with gain embedded in the gap (orange), (b) the retrieved μ with and without the gain material, and (c) the retrieved refractive index.

and to enhance the absorption in the near-infrared. In [133], the authors proposed un-doped monolayer graphene on the top of a photonic crystal slab with cylindrical holes in a silicon sheet to reduce the loss and to enhance graphene absorption in the near-infrared. The active gain medium was filled in the holes, which was utilized as a tunable element for realizing high absorption efficiency. The effect of the active gain on the absorption properties of various deep subwavelength plasmonic materials, including metallic nanoparticles and graphene nanoribbon, was investigated theoretically and numerically in [134].

Although this method provides a very low loss approaching zero with proper gain materials, and maintains the negativity of the constitutive parameters, there is a difficulty in finding suitable materials for achieving the adequate gain. There are also other challenges, such as the complexity of implementation, which requires an equipped laboratory, and high fabrication cost due to the nature and variety of the gain materials. Table 3 summarizes metamaterial loss compensation based on gain materials technique.

D. METAMATERIAL LOSS REDUCTION BASED ON COMPUTATIONAL OPTIMIZATION TECHNIQUES

Computational optimization techniques, such as genetic algorithms (GAs) and particle swarm optimization (PSO), were proposed to optimize the metamaterials and obtain the desired behavior [135], [136]. GA is an artificial intelligence algorithm often utilized to optimize electromagnetic devices in a global sense [137]. The employment of GA for optimizing metamaterials has been fostered in the literature, in particular, to obtain the desired response, such as near-zero constitutive parameters [138], acoustic lens [139], ultra-broadband perfect absorbers [140]. Further, it can determine the number of layers needed for the desired response [141]. PSO is another nature-inspired algorithm introduced by Kennedy and Eberhart in 1995 [142], [143]. This algorithm operates by mimicking social phenomena, in particular, the behaviour of a swarm of individuals (referred to as

TABLE 3. Summary of metamaterial loss compensation based on gain materials technique.

Ref.	Metamaterial shape	Frequency band	Gain material	The measures of the loss
[121]	Silver double fishnet	Visible wavelength 710 nm	Dye molecules	Transmission, imaginary refractive index, and FOM
[124]	Silver rods with QDs	Telecommunication wavelength 1.55 μm	InAs/GaAs QDs	The imaginary value of the ε
[125]	Fishnet with QDs	Telecommunication wavelength 1.5 μm	PbS QDs	Transmission and imaginary values of the ε and μ
[126]	Silver SRR	Telecommunication wavelength 1.5 μm	InGaAs single quantum well	Transmission
[127]	Silver-based SRR	Terahertz regime 100 THz	Isotropic gain, isotropic gain with a shadow cast by the SRR, and anisotropic gain	The imaginary value of the μ
[128]	SRR	Terahertz regime 100 THz	Electric gain	The imaginary values of the μ and the refractive index
[130]	SRR and wire	Microwave regime 10.75 GHz	Niobium (Nb) with different degrees of temperature	Transmission

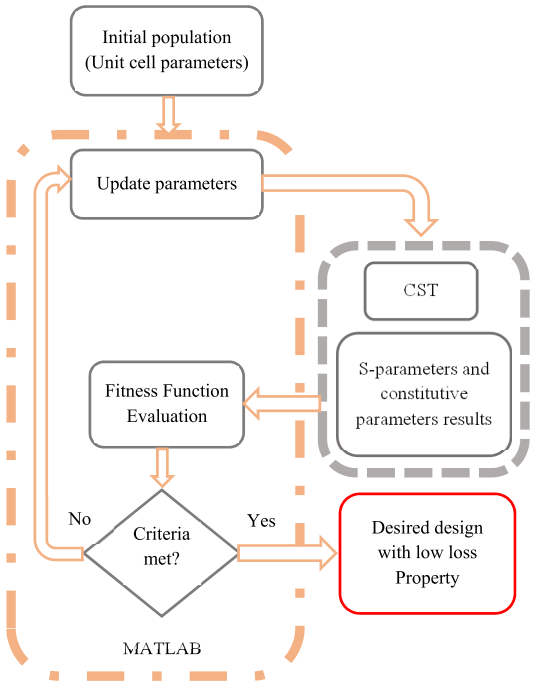

FIGURE 22. The flow chart of the loss optimization based on GA technique.

particles), which are being relocated over the parameter space pertinent to the problem at hand. The first use of PSO in the electromagnetic field was by Rahmat-Samii and Robinson in 2003 [144]. The metamaterials resonant frequency can be optimized by employing PSO, thereby controlling their constitutive parameters. PSO was utilized in [145] to optimize the resonant frequency and constitutive parameters of the SRR structure, thereby enhancing the performance of the fractal antenna. The full-wave simulation tools, such as Computer Simulation Technology (CST) and High-Frequency Structure Simulator (HFSS), are used to design the initial structure. On the other hand, the software development tool, Matlab, is utilized to implement the GA and PSO. These two environments combined to carry out the optimization process. Figure 22 shows the flowchart of the metamaterial loss optimization process based on the GA method. In the literature, both PSO and GA were employed to obtain low loss metamaterials [146]–[152]. A particular focus will be put on the GA because of its popularity in optimizing metamaterials. Bossard *et al.*. [146], [147] proposed two and five cascade metamaterial unit cells to optimize the loss at the terahertz regime. GA was employed to achieve a low loss and maintain the negative refractive index. The transmission spectra and the refractive index were studied to explain the low loss property. The losses of 2.34 dB and 3.2 dB were obtained in [146] and [147], respectively. In [148], the fishnet metamaterial stacks with two metal screens (thin) and five metal screens (thick) were optimized by GA at mid-infrared. The metal screens for both designs were silver (Ag) separated by polyimide layers. The configurations of the thin and thick metamaterials are shown in Figs. 23(a) and (b), respectively. The two and five metal screens achieve transmission losses of 1.1 dB at 2.93 μm and 1.1 dB at 2.86 μm, respectively [see Figs. 23(c) and (d)]. The imaginary refractive index was approached zero for both designs, as displayed in Figs. 23(e) and (f). At the visible spectrum, Kwon and Werner optimized the parameters of the doubly periodic metamaterial by GA for achieving a low loss property [149]. This report demonstrated low loss of 0.5 dB at 0.69 μm. Further, the negative constitutive parameters were provided to support the low loss property. At the microwave regime, Chen *et al.*. [150], used the GA to design magnetic metamaterial with negative μ. The optimized structure provided low loss demonstrated by the low value of the imaginary μ. On the other hand, the PSO was used to optimize the optical metamaterial loss [37], [152]. The transmittance spectra, imaginary refractive index, and FOM were studied to show the low loss behavior. The performance of the PSO was compared to GA, in the favour of the former. The main advantage of this approach is to reduce

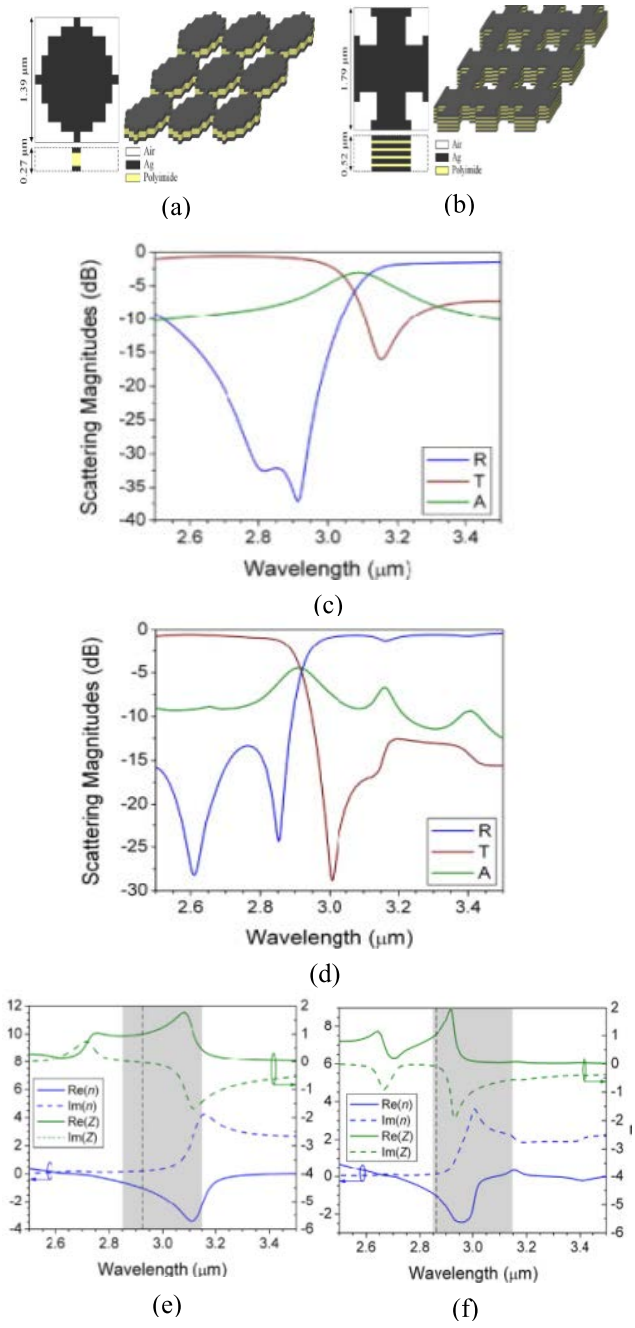

FIGURE 23. Low loss metamaterial based on the GA optimization [148]: (a) and (b) the geometry of single unit cell and periodic structure of the two and five metal screens metamaterials, reflection, transmission, and absorption of the (c) two metal screens and (d) five metal screens, and the refractive index and the impedance of the (e) two metal screens, and (f) five metal screens.

the computational time expenditures required to achieve low loss. Further, it is a systematic process with clear steps that need to be followed. However, it is also considered a complex process and not universal as only few reports discussed this approach in the literature, according to [37]. Table 4 presents the comparison between the available loss reduction approaches. The review accomplished in this work leads to various observations concerning the metamaterial losses and their effects on constructing the functional devices. The following key aspects should be highlighted:

- The inherent losses and narrow bandwidth are the significant challenges that need to be addressed in the metamaterials field, where both can seriously limit their practical applications. High losses are the main barrier in designing efficient metamaterial devices. Such losses restrict the application of metamaterial cloaks and cause difficulties in achieving perfect imaging and absorbers. Their reduction is instrumental in the development of high-performance devices based on metamaterials.
- All loss sources, ohmic, resonant, and radiation, should be considered when designing functional devices of metamaterials. The metal used in the conducting layers is not ideal, especially at the high-frequency range. Thus, the intrinsic or ohmic loss is crucial and must be addressed in the design stage. The inherent losses are not limited to those caused by the conducting layers, where other loss sources include the resonant and radiation ones. The resonant loss is induced by increasing the operating frequency to a higher range. On the other hand, the radiation loss, the dominant component of the losses, is due to the metamaterial elements scattering the electromagnetic waves away from the incident wave. The designer's awareness of all loss sources can help construct high-performance metamaterial devices.
- The available approaches to alleviate/compensate the losses and their performance comparison were discussed in detail to help the designers of the metamaterial devices choose the suitable loss mitigation method. The loss mitigation approach can be determined by several factors: the design simplicity/complexity, the time required for obtaining the desired performance, and fabrication and verification requirements (the cost and availability of the materials and test equipment). A complete comparison of the available techniques highlighting their advantages and drawbacks was provided, which can be used as a guideline for designing low-loss metamaterial devices.
- The microwave regime is the most studied part across the spectra for demonstrating low loss metamaterials. This is due to the availability of materials and equipment for fabrication and measurement in most laboratories. Further, the operation frequency for most metamaterial applications, especially the functional devices, is within this band. On the other hand, a limited number of published works at the high-frequency range (the millimeter-wave and terahertz spectra) is due to fabrication and measurement limitations. Based on the available literature and solutions, the loss mitigation associated with these bands was discussed. The millimeter-wave and terahertz spectrums have recently gained considerable attention due to their large bandwidth, which is a superior feature for delivering the fifth generation (5G) and sixth generation (6G) technologies. Here, the low loss metamaterials are

TABLE 4. Benefits and drawbacks of the loss reduction approaches.

Ref.	Loss reduction approaches	Benefits	drawbacks
[64]–[75] [81]–[95]	EIT	• Low loss. • Low fabrication cost. • Simple implementation.	• Requires a coupling between the bright and dark modes. • Some designs lose the negativity in the real part of constitutive parameters. • The narrow bandwidth of low loss.
[56],[57] [96]–[116]	Geometric tailoring	• Acceptable low loss. • Low fabrication cost. • With proper design, a wide bandwidth of low loss can be obtained.	• It is based on human intuition and has no systematic procedures for obtaining low loss. • It is a time-consuming and not systematic approach compared to other methods.
[120]–[127] [128]–[132]	Gain materials	• Very low loss approaching zero with including proper gain materials. • Maintains the negativity of the constitutive parameters.	• The difficulty of finding suitable material for achieving an adequate gain. • Complex implementation (need an equipped lab.). • High fabrication cost. • Requires an external excitation source.
[146]–[152]	Computational optimization techniques	• Low loss. • Reduce the time consuming for obtaining the low loss. • Systematic approach.	• Complex implementation requires two tools (CST/HFSS and Matlab) to cooperate to achieve the desired response. • Not a common approach where only a few reports discussed this method in the literature.

instrumental in implementing the practical devices for the current 5G (millimeter-wave) and future 6G (terahertz). The construction of metamaterial devices with low loss behavior at these bands would require more investigation either by using the available or even novel approaches to fulfill the requirements of future technologies.

V. CONCLUSION

This review recalled the concept of metamaterials and discussed their applications in constructing variety of functional devices, e.g., absorbers, imaging resolution, and invisibility cloaks. Nevertheless, inherent losses affect their performance and postpone achieving devices-based metamaterials, especially in the high-frequency range. The loss sources, ohmic, resonant, and radiation, were discussed, and their contribution to the loss strength was demonstrated. Four approaches for loss compensation were highlighted based on the available literature at different frequency bands, including EIT, geometric tailoring, embedding gain materials, and computational optimization techniques. The principle of EIT for designing EIT-like metamaterial and including gain materials are systematic and universal approaches, which are considered the most effective techniques for obtaining low losses at different frequency spectra. These techniques result in losses close to zero. On the other hand, geometric tailoring based on human intuition was also reviewed in detail. Although this method also provides acceptable loss levels, it is a time-consuming and not systematic as compared to other methods. The optimization-based loss reduction using, e.g., GA or PSO, is another promising approach to demonstrate low loss structures. Nevertheless, it is not a common approach with only a few reports discussing this method in the literature. The comparison between loss reduction approaches was introduced by highlighting the advantages and drawbacks of each technique.

As a final remark, from our perspective, the current approaches would require more investigation for the field to reach maturity and for metamaterial to have an active involvement in the construction of functional devices, thus penetrating the world markets. Ultimately, we believe that this work can serve as an inspiration and reference point in developing low loss metamaterials to enable a broad range of high-performance devices.

APPENDIX

NOMENCLATURE

EIT	Electromagnetically induced transparency
PSO	Particle swarm optimization
GA	Genetic algorithm
ε	Permittivity
μ	Permeability
SRR	Split-ring resonators
ε_{eff}	Effective permittivity
μ_{eff}	Effective permeability
FOM	Figures of merit
Q-factor	Quality factor
ASRR	Asymmetric split range resonator
DSRR	Double-split ring resonator
SqRR	Square ring resonator
CTCs	Cylindrical through-hole cubes

MDSRR	Modified double square ring resonator
DSRR	Double-gap split ring resonator
SR	Spiral resonator
DBS	Double bowknot-shaped structure
CSSRR	Circular spiral split ring resonator
ASSR	Adjacent square-shaped resonator
CMM	Chiral Metamaterials
FCMM	Fishnet chiral metamaterial
PCBs	Printed circuit boards
ZIMs	Zero index metamaterials
DER	E-shaped resonator
TUSR	T-U shaped resonator
CMM	Composite metamaterial medium
SHR	Semi H-shaped resonator
QDs	Quantum dots
InAs	Indium arsenide
GaAs	Gallium arsenide
PbS	Lead sulfide
CST	Computer Simulation Technology
HFSS	High-Frequency Structure Simulator
Ag	Silver
5G	Fifth generation
6G	Sixth generation

REFERENCES

[1] A. Wegrowski, W.-C. Wang, and C. Tsui, "Three cases of discontinuous refractive index in metamaterial study," *Sci. Rep.*, vol. 12, no. 1, pp. 1–15, Dec. 2022.
[2] S. Zhang, W. Fan, N. C. Panoiu, K. J. Malloy, R. M. Osgood, and S. R. J. Brueck, "Experimental demonstration of near-infrared negative-index metamaterials," *Phys. Rev. Lett.*, vol. 95, no. 13, pp. 1–4, Sep. 2005.
[3] J. B. Pendry, A. J. Holden, D. J. Robbins, and W. J. Stewart, "Magnetism from conductors and enhanced nonlinear phenomena," *IEEE Trans. Microw. Theory Techn.*, vol. 47, no. 11, pp. 2075–2084, Nov. 1999.
[4] B. Nguyen, N. Phu, V. Sau, N. Cong, and D. Le Van, "Negative refractive index in an inhomogeneously broadened four-level inverted-Y atomic medium," *IEEE Photon. J.*, vol. 13, no. 6, pp. 1–7, Dec. 2021.
[5] S. L. Zhai, X. P. Zhao, S. Liu, F. L. Shen, L. L. Li, and C. R. Luo, "Inverse Doppler effects in broadband acoustic metamaterials," *Sci. Rep.*, vol. 6, no. 1, pp. 1–10, Sep. 2016.
[6] Z. Duan, X. Tang, Z. Wang, Y. Zhang, X. Chen, M. Chen, and Y. Gong, "Observation of the reversed Cherenkov radiation," *Nature Commun.*, vol. 8, no. 1, pp. 1–7, Apr. 2017.
[7] R. A. Shelby, D. R. Smith, and S. Schultz, "Experimental verification of a negative index of refraction," *Science*, vol. 292, no. 5514, pp. 77–79, Apr. 2001.
[8] V. G. Veselago, "The electrodynamic of substances with simultaneous negative values of ϵ and μ," *Sov. Phys. Uspekhi*, vol. 10, no. 4, pp. 509–514, 1968.
[9] J. B. Pendry, A. J. Holden, W. J. Stewart, and I. Youngs, "Extremely low frequency plasmons in metallic mesostructures," *Phys. Rev. Lett.*, vol. 76, no. 25, pp. 4773–4776, Jun. 1996.
[10] D. R. Smith, W. J. Padilla, D. C. Vier, S. C. Nemat-Nasser, and S. Schultz, "Composite medium with simultaneously negative permeability and permittivity," *Phys. Rev. Lett.*, vol. 84, pp. 4184–4187, May 2000.
[11] Z. Manzoor, "Aperiodic hyperbolic metamaterial superlens with random distribution," *Optik*, vol. 242, Sep. 2021, Art. no. 167290.
[12] S. Mukherjee, Z. Su, L. Udpa, S. Udpa, and A. Tamburrino, "Enhancement of microwave imaging using a metamaterial lens," *IEEE Sensors J.*, vol. 19, no. 13, pp. 4962–4971, Jul. 2019.
[13] D. Ramaccia, D. L. Sounas, A. Alú, F. Bilotti, and A. Toscano, "Nonreciprocity in antenna radiation induced by space-time varying metamaterial cloaks," *IEEE Antennas Wireless Propag. Lett.*, vol. 17, no. 11, pp. 1968–1972, Sep. 2018.
[14] H. K. Zhang, Y. Chen, X. N. Liu, and G. K. Hu, "An asymmetric elastic metamaterial model for elastic wave cloaking," *J. Mech. Phys. Solids*, vol. 135, pp. 1–12, Feb. 2020.
[15] Y. Luo, N. Dong, Y. Pei, F. Qian, R. Wang, H. Cui, G. Yang, and X. Hu, "A sensitive glucose sensor based on active metamaterial with programmable states," *IEEE Sensors J.*, vol. 21, no. 21, pp. 24038–24047, Nov. 2021.
[16] E. Celenk and N. T. Tokan, "Frequency scanning conformal sensor based on SIW metamaterial antenna," *IEEE Sensors J.*, vol. 21, no. 14, pp. 16015–16023, Jul. 2021.
[17] A. Mohanty, O. P. Acharya, B. Appasani, S. K. Mohapatra, and M. S. Khan, "Design of a novel terahertz metamaterial absorber for sensing applications," *IEEE Sensors J.*, vol. 21, no. 20, pp. 22688–22694, Oct. 2021.
[18] Y.-H. Ke, L.-L. Yang, Y.-Y. Zhu, J. Wang, and J.-X. Chen, "Filtering quasi-Yagi strip-loaded DRR antenna with enhanced gain and selectivity by metamaterial," *IEEE Access*, vol. 9, pp. 31755–31761, 2021.
[19] A. K. Vallappil, M. K. A. Rahim, B. A. Khawaja, and M. N. Iqbal, "Compact metamaterial based 4 × 4 Butler matrix with improved bandwidth for 5G applications," *IEEE Access*, vol. 8, pp. 13573–13583, 2020.
[20] B. A. F. Esmail, S. Koziel, and S. Szczepanski, "Overview of planar antenna loading metamaterials for gain performance enhancement: The two decades of progress," *IEEE Access*, vol. 10, pp. 27381–27403, 2022.
[21] Z. Wani, M. P. Abegaonkar, and S. K. Koul, "High-low-epsilon biaxial anisotropic lens for enhanced gain and aperture efficiency of a linearly polarized antenna," *IEEE Trans. Antennas Propag.*, vol. 68, no. 12, pp. 8133–8138, Dec. 2020.
[22] S. Liu, Z. Wang, and Y. Dong, "Compact wideband SRR-inspired antennas for 5G microcell applications," *IEEE Trans. Antennas Propag.*, vol. 69, no. 9, pp. 5998–6003, Sep. 2021.
[23] B. A. F. Esmail, H. A. Majid, S. H. Dahlan, Z. Z. Abidin, M. Himdi, R. Dewan, M. K. A. Rahim, and A. Y. I. Ashyap, "Reconfigurable metamaterial structure for 5G beam tilting antenna applications," *Waves Random Complex Media*, vol. 31, no. 6, pp. 2089–2102, Nov. 2021.
[24] L. Zhu, F.-Y. Meng, L. Dong, J.-H. Fu, and Q. Wu, "Low-loss magnetic metamaterial at THz frequencies by suppressing radiation losses," *IEEE Trans. THz Sci. Technol.*, vol. 3, no. 6, pp. 805–811, Nov. 2013.
[25] B. A. F. Esmail, H. A. Majid, Z. Z. Abidin, S. H. Dahlan, M. Himdi, R. Dewan, M. K. Rahim, and N. Al-Fadhali, "Reconfigurable radiation pattern of planar antenna using metamaterial for 5G applications," *Materials*, vol. 13, no. 3, pp. 1–15, 2020.
[26] K. L. Tsakmakidis, M. S. Wartak, J. J. H. Cook, J. M. Hamm, and O. Hess, "Negative-permeability electromagnetically induced transparent and magnetically active metamaterials," *Phys. Rev. B, Condens. Matter*, vol. 81, no. 19, pp. 1–11, May 2010.
[27] A. Boltasseva and H. A. Atwater, "Low-loss plasmonic metamaterials," *Mater. Sci.*, vol. 331, no. 6015, pp. 290–291, Jan. 2011.
[28] T. Q. Li, H. Liu, T. Li, S. M. Wang, J. X. Cao, Z. H. Zhu, Z. G. Dong, S. N. Zhu, and X. Zhang, "Suppression of radiation loss by hybridization effect in two coupled split-ring resonators," *Phys. Rev. B, Condens. Matter*, vol. 80, no. 11, pp. 1–18, Sep. 2009.
[29] F. Y. Meng, J. H. Fu, K. Zhang, Q. Wu, J. Y. Kim, J. J. Choi, B. Lee, and J. C. Lee, "Metamaterial analogue of electromagnetically induced transparency in two orthogonal directions," *J. Phys. D, Appl. Phys.*, vol. 44, no. 26, pp. 1–7, 2011.
[30] L. Zhu, F. Y. Meng, J. H. Fu, and Q. Wu, "An electromagnetically induced transparency metamaterial with polarization insensitivity based on multi-quasi-dark modes," *J. Phys. D, Appl. Phys.*, vol. 45, no. 44, pp. 1–6, 2012.
[31] L. Zhu, L. Dong, F.-Y. Meng, J.-H. Fu, and Q. Wu, "Influence of symmetry breaking in a planar metamaterial on transparency effect and sensing application," *Appl. Opt.*, vol. 51, no. 32, p. 7794, 2012.
[32] A. D. Boardman and K. Marinov, "Radiation enhancement and radiation suppression by a left-handed metamaterial," *Microw. Opt. Technol. Lett.*, vol. 48, no. 12, pp. 2512–2516, 2006.
[33] L. Zhu, F.-Y. Meng, F. Zhang, J. Fu, Q. Wu, X. M. Ding, and J. L.-W. Li, "An ultra-low loss split ring resonator by suppressing the electric dipole moment approach," *Prog. Electromagn. Res.*, vol. 137, pp. 239–254, 2013.

[34] Z. H. Jiang, S. Yun, L. Lin, J. A. Bossard, D. H. Werner, and T. S. Mayer, "Tailoring dispersion for broadband low-loss optical metamaterials using deep-subwavelength inclusions," *Sci. Rep.*, vol. 3, no. 1, pp. 1–9, Dec. 2013.

[35] Y. Fan, Z. Wei, H. Li, H. Chen, and C. M. Soukoulis, "Low-loss and high-Q planar metamaterial with toroidal moment," *Phys. Rev. B, Condens. Matter*, vol. 87, no. 11, pp. 1–5, Mar. 2013.

[36] A. D. Boardman, V. V. Grimalsky, Y. S. Kivshar, S. V. Koshevaya, M. Lapine, N. M. Litchinitser, V. N. Malnev, M. Noginov, Y. G. Rapoport, and V. M. Shalaev, "Active and tunable metamaterials," *Laser Photon. Rev.*, vol. 5, no. 2, pp. 287–307, 2011.

[37] A. V. Kildishev, U. K. Chettiar, Z. Liu, V. M. Shalaev, D. H. Kwon, Z. Bayraktar, and D. H. Werner, "Stochastic optimization of low-loss optical negative-index metamaterial," *J. Opt. Soc. Amer. B, Opt. Phys.*, vol. 24, no. 10, pp. 34–39, 2007.

[38] C. Milias, R. B. Andersen, P. I. Lazaridis, Z. D. Zaharis, B. Muhammad, J. T. B. Kristensen, A. Mihovska, and D. D. S. Hermansen, "Metamaterial-inspired antennas: A review of the state of the art and future design challenges," *IEEE Access*, vol. 9, pp. 89846–89865, 2021.

[39] S. Xiao, T. Wang, T. Liu, C. Zhou, X. Jiang, and J. Zhang, "Active metamaterials and metadevices: A review," *J. Phys. D, Appl. Phys.*, vol. 53, no. 50, Dec. 2020, Art. no. 503002.

[40] T. Koschny, M. Kafesaki, E. N. Economou, and C. M. Soukoulis, "Effective medium theory of left-handed materials," *Phys. Rev. Lett.*, vol. 93, no. 10, pp. 1–4, Sep. 2004.

[41] X. Fu and T. J. Cui, "Recent progress on metamaterials: From effective medium model to real-time information processing system," *Prog. Quantum Electron.*, vol. 67, pp. 1–38, Sep. 2019.

[42] X. Chen, T. M. Grzegorczyk, B.-I. Wu, J. Pacheco, and J. A. Kong, "Robust method to retrieve the constitutive effective parameters of metamaterials," *Phys. Rev. E, Stat. Phys. Plasmas Fluids Relat. Interdiscip. Top.*, vol. 70, no. 1, pp. 1–7, Jul. 2004.

[43] D. R. Smith, D. C. Vier, T. Koschny, and C. M. Soukoulis, "Electromagnetic parameter retrieval from inhomogeneous metamaterials," *Phys. Rev. E, Stat. Phys. Plasmas Fluids Relat. Interdiscip. Top.*, vol. 71, no. 3, pp. 1–11, Mar. 2005.

[44] J. B. Pendry, D. Schurig, and D. R. Smith, "Controlling electromagnetic fields," *Science*, vol. 312, pp. 1780–1782, Jun. 2006.

[45] D. Schurig, J. J. Mock, B. J. Justice, S. A. Cummer, J. B. Pendry, A. F. Starr, and D. R. Smith, "Metamaterial electromagnetic cloak at microwave frequencies," *Science*, vol. 314, no. 5801, pp. 977–980, Oct. 2006.

[46] J. B. Pendry, "Negative refraction makes a perfect lens," *Phys. Rev. Lett.*, vol. 85, no. 18, pp. 3966–3969, Oct. 2000.

[47] A. Grbic and G. V. Eleftheriades, "Overcoming the diffraction limit with a planar left-handed transmission-line lens," *Phys. Rev. Lett.*, vol. 92, no. 11, pp. 1–4, Mar. 2004.

[48] N. I. Landy, S. Sajuyigbe, J. J. Mock, D. R. Smith, and W. J. Padilla, "Perfect metamaterial absorber," *Phys. Rev. Lett.*, vol. 100, no. 20, pp. 1–4, 2008.

[49] S. Liu, H. Chen, and T. J. Cui, "A broadband terahertz absorber using multi-layer stacked bars," *Appl. Phys. Lett.*, vol. 106, no. 15, pp. 1–6, 2015.

[50] Z. Xiao, Q. Xu, and C. Li, "Metamaterial bandpass filter based on three-dimensional structure," *J. Electron. Mater.*, vol. 50, no. 8, pp. 4358–4363, Aug. 2021.

[51] H. Yao, H. Mei, W. Zhang, S. Zhong, and X. Wang, "Theoretical and experimental research on terahertz metamaterial sensor with flexible substrate," *IEEE Photon. J.*, vol. 14, no. 1, pp. 1–9, Feb. 2022.

[52] F. Li, H. Chen, Q. He, Y. Zhou, L. Zhang, X. Weng, H. Lu, J. Xie, and L. Deng, "Design and implementation of metamaterial polarization converter with the reflection and transmission polarization conversion simultaneously," *J. Opt.*, vol. 21, no. 4, pp. 1–9, 2019.

[53] J. Yang, M. Huang, C. Yang, Z. Xiao, and J. Peng, "Metamaterial electromagnetic concentrators with arbitrary geometries," *Opt. Exp.*, vol. 17, no. 22, pp. 19656–19661, 2010.

[54] Y. S. Choudhary and N. Gomathi, "Metamaterials as shielding materials," in *Advanced Materials for Electromagnetic Shielding: Fundamentals, Properties, and Applications*. Hoboken, NJ, USA: Wiley, 2018, pp. 367–391.

[55] M. Luo, X. Sang, J. Tan, and J. Chen, "A novel miniaturized metamaterial lens antenna," *Int. J. RF Microw. Comput.-Aided Eng.*, vol. 30, no. 7, pp. 1–8, Jul. 2020.

[56] D. Ö. Güney, T. Koschny, and C. M. Soukoulis, "Reducing ohmic losses in metamaterials by geometric tailoring," *Phys. Rev. B, Condens. Matter*, vol. 80, no. 12, pp. 1–16, Sep. 2009.

[57] J. Zhou, T. Koschny, and C. M. Soukoulis, "An efficient way to reduce losses of left-handed metamaterials," *Opt. Exp.*, vol. 16, no. 15, pp. 11147–11152, 2008.

[58] L. Zhu, F.-Y. Meng, J.-H. Fu, Q. Wu, and J. Hua, "An approach to configure low-loss and full transmission metamaterial based on electromagnetically induced transparency," *IEEE Trans. Magn.*, vol. 48, no. 11, pp. 4285–4288, Nov. 2012.

[59] T. Cao, C. Wei, and M. J. Cryan, "Low-loss dual-band double-negative chirped metamaterial," *J. Opt. Soc. Amer. B, Opt. Phys.*, vol. 32, no. 1, pp. 108–113, 2015.

[60] G. Dolling, C. Enkrich, M. Wegener, C. M. Soukoulis, and S. Linden, "Low-loss negative-index metamaterial at telecommunication wavelengths," *Opt. Lett.*, vol. 31, no. 12, pp. 1800–1802, Jun. 2006.

[61] X. Liu, J. Gu, R. Singh, Y. Ma, J. Zhu, Z. Tian, M. He, J. Han, and W. Zhang, "Electromagnetically induced transparency in terahertz plasmonic metamaterials via dual excitation pathways of the dark mode," *Appl. Phys. Lett.*, vol. 100, no. 13, pp. 2010–2014, 2012.

[62] B. A. F. Esmail, "Pattern reconfigurable metamaterial antenna for 5G base station network," Ph.D. dissertation, Dept. Commun. Eng., UTHM, Johor, Malaysia, 2021.

[63] Z. Li, Y. Ma, R. Huang, R. Singh, J. Gu, Z. Tian, J. Han, and W. Zhang, "Manipulating the plasmon-induced transparency in terahertz metamaterials," *Opt. Exp.*, vol. 19, no. 9, pp. 8912–8919, Apr. 2011.

[64] H. M. Li, S. B. Liu, S. Y. Liu, S. Y. Wang, G. W. Ding, H. Yang, Z. Y. Yu, and H. F. Zhang, "Low-loss metamaterial electromagnetically induced transparency based on electric toroidal dipolar response," *Appl. Phys. Lett.*, vol. 106, no. 8, pp. 1–5, 2015.

[65] Y. Fan, T. Qiao, F. Zhang, Q. Fu, J. Dong, B. Kong, and H. Li, "An electromagnetic modulator based on electrically controllable metamaterial analogue to electromagnetically induced transparency," *Sci. Rep.*, vol. 7, no. 1, pp. 1–7, Mar. 2017.

[66] L. Zhang, P. Tassin, T. Koschny, C. Kurter, S. M. Anlage, and C. M. Soukoulis, "Large group delay in a microwave metamaterial analog of electromagnetically induced transparency," *Appl. Phys. Lett.*, vol. 97, no. 24, pp. 1–4, 2010.

[67] Y. Tian, S. Hu, X. Huang, Z. Yu, H. Lin, and H. Yang, "Low-loss planar metamaterials electromagnetically induced transparency for sensitive refractive index sensing," *J. Phys. D, Appl. Phys.*, vol. 50, no. 40, pp. 1–21, 2017.

[68] Y. Sun, H. Jiang, Y. Yang, Y. Zhang, H. Chen, and S. Zhu, "Electromagnetically induced transparency in metamaterials: Influence of intrinsic loss and dynamic evolution," *Phys. Rev. B, Condens. Matter*, vol. 83, no. 19, pp. 1–6, May 2011.

[69] L. Zhu, L. Dong, J. Guo, F.-Y. Meng, X. J. He, C. H. Zhao, and Q. Wu, "A low-loss electromagnetically induced transparency (EIT) metamaterial based on coupling between electric and toroidal dipoles," *RSC Adv.*, vol. 7, no. 88, pp. 55897–55904, 2017.

[70] L. Zhu, F. Y. Meng, L. Dong, Q. Wu, B. J. Che, J. Gao, J. H. Fu, K. Zhang, and G. H. Yang, "Magnetic metamaterial analog of electromagnetically induced transparency and absorption," *J. Appl. Phys.*, vol. 117, no. 17, pp. 1–5, 2015.

[71] T. Xiang, T. Lei, S. Hu, J. Chen, X. Huang, and H. Yang, "Resonance transparency with low-loss in toroidal planar metamaterial," *J. Appl. Phys.*, vol. 123, no. 9, Mar. 2018, Art. no. 095104.

[72] F. Bagci and B. Akaoglu, "Transmission control by asymmetric electromagnetically induced transparency-like metamaterials in transverse electromagnetic waveguide," *Phys. Lett. A*, vol. 383, no. 35, Dec. 2019, Art. no. 126000.

[73] L. Zhu, X. Zhao, C. Zhao, L. Dong, F. J. Miao, C. H. Wang, and J. Guo, "Low loss and high transmission electromagnetically induced transparency (EIT) effect in cylindrical through-hole dielectric cubes," *Prog. Electromagn. Res. M*, vol. 76, pp. 207–215, 2018.

[74] L. Zhu, X. Zhao, F. J. Miao, B. K. Ghosh, L. Dong, B. R. Tao, F. Y. Meng, and W. N. Li, "Dual-band polarization convertor based on electromagnetically induced transparency (EIT) effect in all-dielectric metamaterial," *Opt. Exp.*, vol. 27, no. 9, p. 12163, 2019.

[75] Z.-Y. Shen, H.-L. Yang, X. Liu, X.-J. Huang, T.-Y. Xiang, J. Wu, and W. Chen, "Electromagnetically induced transparency in novel dual-band metamaterial excited by toroidal dipolar response," *Frontiers Phys.*, vol. 15, no. 1, pp. 1–7, Feb. 2020.

[76] W. Kamonsin, P. Krachodnok, P. Chomtong, and P. Akkaraekthalin, "Dual-band metamaterial based on Jerusalem cross structure with interdigital technique for LTE and WLAN systems," *IEEE Access*, vol. 8, pp. 21565–21572, 2020.
[77] I. A. Mocanu, "Compact dual band ring coupler using miniaturized metamaterial left-handed impedance inverters," *IEEE Access*, vol. 9, pp. 86119–86131, 2021.
[78] A. K. Singh, M. P. Abegaonkar, and S. K. Koul, "Dual- and triple-band polarization insensitive ultrathin conformal metamaterial absorbers with wide angular stability," *IEEE Trans. Electromagn. Compat.*, vol. 61, no. 3, pp. 878–886, Jun. 2019.
[79] A. Vahidi, H. Rajabalipanah, A. Abdolali, and A. Cheldavi, "A honeycomb-like three-dimensional metamaterial absorber via super-wideband and wide-angle performances at millimeter wave and low THz frequencies," *Appl. Phys. A, Solids Surf.*, vol. 124, no. 4, pp. 1–10, Apr. 2018.
[80] Z. Tao, D. Bao, H. X. Xu, H. F. Ma, W. X. Jiang, and T. J. Cui, "A millimeter-wave system of antenna array and metamaterial lens," *IEEE Antennas Wireless Propag. Lett.*, vol. 15, pp. 370–373, 2016.
[81] B. A. Esmail, H. B. Majid, Z. B. Z. Abidin, S. H. B. Dahlan, M. Himdi, M. R. Kamarudin, and M. K. Rahim, "Dual mode modified double square ring resonator structure at 76 GHz," *Microw. Opt. Technol. Lett.*, vol. 61, no. 7, pp. 1678–1682, Jul. 2019.
[82] J. Xie, X. Zhu, X. Zang, Q. Cheng, Y. Ye, and Y. Zhu, "High extinction ratio electromagnetically induced transparency analogue based on the radiation suppression of dark modes," *Sci. Rep.*, vol. 7, no. 1, pp. 1–8, Dec. 2017.
[83] B. A. F. Esmail, H. A. Majid, F. A. Saparudin, M. Jusoh, A. Y. Ashyap, N. Al-Fadhali, and M. K. A. Rahim, "Negative refraction metamaterial with low loss property at millimeter wave spectrum," *Bull. Electr. Eng. Informat.*, vol. 9, no. 3, pp. 1038–1045, Jun. 2020.
[84] Y. Zhang, J. Wu, L. Liang, G. Zhou, F. Zheng, C. Li, C. Zhang, and B. Jin, "Tailoring electromagnetically induced transparency effect of terahertz metamaterials on ultrathin substrate," *Sci. China Inf. Sci.*, vol. 59, no. 4, pp. 1–6, Apr. 2016.
[85] P. Tassin, L. Zhang, T. Koschny, E. N. Economou, and C. M. Soukoulis, "Low-loss metamaterials based on classical electromagnetically induced transparency," *Phys. Rev. Lett.*, vol. 102, no. 5, pp. 1–5, Feb. 2009.
[86] F.-Y. Meng, F. Zhang, K. Zhang, Q. Wu, J.-Y. Kim, J.-J. Choi, B. Lee, and J.-C. Lee, "Low-loss magnetic metamaterial based on analog of electromagnetically induced transparency," *IEEE Trans. Magn.*, vol. 47, no. 10, pp. 3347–3350, Oct. 2011.
[87] J. Hu, T. Lang, W. Xu, J. Liu, and Z. Hong, "Experimental demonstration of electromagnetically induced transparency in a conductively coupled flexible metamaterial with cheap aluminum foil," *Nanosc. Res. Lett.*, vol. 14, no. 1, pp. 1–10, Dec. 2019.
[88] T. Liu, H. Wang, Y. Liu, L. Xiao, C. Zhou, Y. Liu, C. Xu, and S. Xiao, "Independently tunable dual-spectral electromagnetically induced transparency in a terahertz metal–graphene metamaterial," *J. Phys. D, Appl. Phys.*, vol. 51, no. 41, Oct. 2018, Art. no. 415105.
[89] S. Zhang, D. A. Genov, Y. Wang, M. Liu, and X. Zhang, "Plasmon-induced transparency in metamaterials," *Phys. Rev. Lett.*, vol. 101, no. 4, pp. 1–4, Jul. 2008.
[90] J. Gu, R. Singh, X. Liu, X. Zhang, Y. Ma, S. Zhang, S. A. Maier, Z. Tian, A. K. Azad, H. T. Chen, A. J. Taylor, J. Han, and W. Zhang, "Active control of electromagnetically induced transparency analogue in terahertz metamaterials," *Nature Commun.*, vol. 3, no. 1, pp. 1–6, 2012.
[91] J. Zhang, S. Xiao, C. Jeppesen, A. Kristensen, and N. A. Mortensen, "Electromagnetically induced transparency in metamaterials at near-infrared frequency," *Opt. Exp.*, vol. 18, no. 16, 2010, Art. no. 17187.
[92] M. Qin, C. Pan, Y. Chen, Q. Ma, S. Liu, E. Wu, and B. Wu, "Electromagnetically induced transparency in all-dielectric U-shaped silicon metamaterials," *Appl. Sci.*, vol. 8, no. 10, p. 1799, Oct. 2018.
[93] B. Han, X. Li, C. Sui, J. Diao, X. Jing, and Z. Hong, "Analog of electromagnetically induced transparency in an E-shaped all-dielectric metasurface based on toroidal dipolar response," *Opt. Mater. Exp.*, vol. 8, no. 8, p. 2197, 2018.
[94] C. Sui, B. Han, T. Lang, X. Li, X. Jing, and Z. Hong, "Electromagnetically induced transparency in an all-dielectric metamaterial-waveguide with large group index," *IEEE Photon. J.*, vol. 9, no. 5, pp. 1–8, Oct. 2017.
[95] Z. Wei, X. Li, N. Zhong, X. Tan, X. Zhang, H. Liu, H. Meng, and R. Liang, "Analogue electromagnetically induced transparency based on low-loss metamaterial and its application in nanosensor and slow-light device," *Plasmonics*, vol. 12, no. 3, pp. 641–647, Jun. 2017.
[96] B. A. F. Esmail, H. A. Majid, Z. Z. Abidin, S. H. Dahlan, and M. K. A. Rahim, "Reconfigurable metamaterial structure at millimeter wave frequency range," *Int. J. Electr. Comput. Eng. (IJECE)*, vol. 7, no. 6, p. 2942, Dec. 2017.
[97] X. Zhou, Y. Liu, and X. Zhao, "Low losses left-handed materials with optimized electric and magnetic resonance," *Appl. Phys. A, Solids Surf.*, vol. 98, no. 3, pp. 643–649, Mar. 2010.
[98] T. Shaw and D. Mitra, "Design of miniaturized, low-loss and flexible multi-band metamaterial for microwave application," *Appl. Phys. A, Solids Surf.*, vol. 124, no. 4, pp. 1–11, Apr. 2018.
[99] B. A. F. Esmail, H. B. Majid, S. H. Dahlan, Z. Z. Abidin, M. K. A. Rahim, and M. Jusoh, "Planar antenna beam deflection using low-loss metamaterial for future 5G applications," *Int. J. RF Microw. Comput.-Aided Eng.*, vol. 29, no. 10, pp. 1–11, Oct. 2019.
[100] B. A. F. Esmail, H. A. Majid, S. H. Dahlan, Z. Z. Abidin, M. K. A. Rahim, M. A. Abdullah, and M. Jusoh, "Antenna beam tilting and gain enhancement using novel metamaterial structure at 28 GHz," in *Proc. IEEE Int. RF Microw. Conf. (RFM)*, Dec. 2018, pp. 53–56.
[101] B. A. F. Esmail, H. A. Majid, M. F. Ismail, S. H. Dahlan, Z. Z. Abidin, and M. K. A. Rahim, "Dual band low loss metamaterial structure at millimetre wave band," *Indones. J. Electr. Eng. Comput. Sci.*, vol. 15, no. 2, pp. 823–830, 2019.
[102] O. Fernandez, A. Gomez, A. Vegas, G. J. Molina-Cuberos, and A. J. Garcia-Collado, "Low-loss left-handed gammadion-fishnet chiral metamaterials," *IEEE Antennas Wireless Propag. Lett.*, vol. 18, no. 10, pp. 2041–2045, Oct. 2019.
[103] J. Sun, L. Kang, R. Wang, L. Liu, L. Sun, and J. Zhou, "Low loss negative refraction metamaterial using a close arrangement of split-ring resonator arrays," *New J. Phys.*, vol. 12, no. 8, pp. 1–8, 2010.
[104] Y. J. Huang, G. J. Wen, T. Q. Li, and K. Xie, "Low-loss, broadband and tunable negative refractive index metamaterial," *J. Electromagn. Anal. Appl.*, vol. 2, no. 2, pp. 104–110, 2010.
[105] J.-W. Ma, X.-Q. Zhu, S. Bi, G.-Y. Bai, and Z.-L. Hou, "Low-loss near-zero-index metamaterial based on a single board for broadband electromagnetic-wave switches," *Opt. Commun.*, vol. 446, pp. 113–117, Sep. 2019.
[106] P. Moitra, Y. Yang, Z. Anderson, I. I. Kravchenko, D. P. Briggs, and J. Valentine, "Realization of an all-dielectric zero-index optical metamaterial," *Nature Photon.*, vol. 7, no. 10, pp. 791–795, Oct. 2013.
[107] Z. He, J. Jin, Y. Zhang, and Y. Duan, "Design of a two-dimensional 'T' shaped metamaterial with wideband, low loss," *IEEE Trans. Appl. Supercond.*, vol. 29, no. 2, pp. 1–4, Mar. 2019.
[108] B. A. F. Esmail, H. A. Majid, S. H. Dahlan, Z. Z. Abidin, M. K. A. Rahim, and R. Dewan, "Novel metamaterial structures with low loss at millimeter wave frequency range," *Indones. J. Electr. Eng. Comput. Sci.*, vol. 10, no. 2, pp. 641–647, 2018.
[109] K. B. Alici and E. Ozbay, "Theoretical study and experimental realization of a low-loss metamaterial operating at the millimeter-wave regime: Demonstrations of flat- and prism-shaped samples," *IEEE J. Sel. Topics Quantum Electron.*, vol. 16, no. 2, pp. 386–393, Mar./Apr. 2010.
[110] T. A. Suzuki, M. A. S. Ekiya, T. A. S. Ato, Y. Uki, and T. Akebayashi, "Negative refractive index metamaterial with high transmission, low reflection, and low loss in the terahertz waveband," *Opt. Exp.*, vol. 26, no. 7, pp. 435–441, 2018.
[111] M. Askari, A. Zakery, and A. S. Jahromi, "A low loss semi H-shaped negative refractive index metamaterial at 4.725 THz," *Photon. Nanostruct. Fundam. Appl.*, vol. 30, pp. 78–83, Jul. 2018.
[112] Z. Geng, X. Guo, Y. Cao, Y. Yang, and H. Chen, "Flexible, low-loss and large area metamaterials with high Q value," *Microelectron. Eng.*, vol. 135, pp. 23–27, Mar. 2015.
[113] M. I. Aslam and D. Güney, "Optimizing low loss negative index metamaterial for visible spectrum using differential evolution: Comment," *Opt. Exp.*, vol. 22, no. 4, pp. 3773–3774, 2014.
[114] S. Iyer, S. Popov, and A. T. Friberg, "Loss optimization in double fishnet metamaterials at telecommunication wavelengths," *J. Eur. Opt. Soc., Rapid Publications*, vol. 6, pp. 1–5, Mar. 2011.

[115] S. Yun, Z. H. Jiang, Q. Xu, Z. Liu, D. H. Werner, and T. S. Mayer, "Low-loss impedance-matched optical metamaterials with zero-phase delay," *ACS Nano*, vol. 6, no. 5, pp. 4475–4482, May 2012.

[116] R. Paniagua-Domínguez, D. R. Abujetas, and J. A. Sánchez-Gil, "Ultra low-loss, isotropic optical negative-index metamaterial based on hybrid metal-semiconductor nanowires," *Sci. Rep.*, vol. 3, no. 1, pp. 1–7, Dec. 2013.

[117] M. A. Noginov, G. Zhu, M. Bahoura, J. Adegoke, and C. E. Small, "Enhancement of surface plasmons in an Agraggregate by optical gain in a dielectric medium," *Opt. Lett.*, vol. 31, no. 20, pp. 3022–3024, 2006.

[118] D. Ye, K. Chang, L. Ran, and H. Xin, "Microwave gain medium with negative refractive index," *Nature Commun.*, vol. 5, no. 1, pp. 1–7, Dec. 2014.

[119] S. Droulias, T. Koschny, M. Kafesaki, and C. M. Soukoulis, "On loss compensation, amplification and lasing in metallic metamaterials," *Nanomater. Nanotechnol.*, vol. 9, pp. 1–12, Jan. 2019.

[120] S. Xiao, V. P. Drachev, A. V. Kildishev, X. Ni, U. K. Chettiar, H. K. Yuan, and V. M. Shalaev, "Loss-free and active optical negative-index metamaterials," *Nature*, vol. 466, pp. 735–738, Aug. 2010.

[121] S. Wuestner, A. Pusch, K. L. Tsakmakidis, J. M. Hamm, and O. Hess, "Gain and plasmon dynamics in active negative-index metamaterials," *Phil. Trans. Roy. Soc. A, Math., Phys. Eng. Sci.*, vol. 369, no. 1950, pp. 3525–3550, Sep. 2011.

[122] C. M. Soukoulis and M. Wegener, "Optical Metamaterials—More bulky and less lossy," *Science*, vol. 330, no. 6011, pp. 1633–1634, Dec. 2010.

[123] M. I. Stockman, "Spaser action, loss compensation, and stability in plasmonic systems with gain," *Phys. Rev. Lett.*, vol. 106, no. 15, pp. 1–4, Apr. 2011.

[124] A. Bratkovsky, E. Ponizovskaya, S.-Y. Wang, P. Holmström, L. Thylén, Y. Fu, and H. Ågren, "A metal-wire/quantum-dot composite metamaterial with negative ε and compensated optical loss," *Appl. Phys. Lett.*, vol. 93, no. 19, Nov. 2008, Art. no. 193106.

[125] Z. G. Dong, H. Liu, T. Li, Z. H. Zhu, S. M. Wang, J. X. Cao, S. N. Zhu, and X. Zhang, "Optical loss compensation in a bulk left-handed metamaterial by the gain in quantum dots Optical," *Appl. Phys. Lett.*, vol. 96, no. 4, pp. 1–3, 2010.

[126] N. Meinzer, M. Ruther, S. Linden, C. M. Soukoulis, G. Khitrova, J. Hendrickson, J. D. Olitzky, H. M. Gibbs, and M. Wegener, "Arrays of Ag split-ring resonators coupled to InGaAs single-quantum-well gain," *Opt. Exp.*, vol. 18, no. 23, pp. 24140–24151, 2010.

[127] A. Fang, Z. Huang, T. Koschny, and C. M. Soukoulis, "Overcoming the losses of a split ring resonator array with gain," *Opt. Exp.*, vol. 19, no. 13, pp. 12688–12699, 2011.

[128] A. Fang, T. Koschny, and C. M. Soukoulis, "Lasing in metamaterial nanostructures," *J. Opt.*, vol. 12, no. 2, pp. 1–18, 2011.

[129] A. Fang, T. Koschny, M. Wegener, and C. M. Soukoulis, "Self-consistent calculation of metamaterials with gain," *Phys. Rev. B, Condens. Matter*, vol. 79, no. 24, pp. 1–4, Jun. 2009.

[130] M. Ricci, N. Orloff, and S. M. Anlage, "Superconducting metamaterials," *Appl. Phys. Lett.*, vol. 87, no. 3, pp. 1–4, 2005.

[131] A. N. Lagarkov, V. N. Kisel, and A. K. Sarychev, "Loss and gain in metamaterials," *J. Opt. Soc. Amer. B, Opt. Phys.*, vol. 27, no. 4, pp. 648–659, 2010.

[132] A. N. Lagarkov and V. N. Kisel, "Losses in metamaterials: Restrictions and benefits," *Phys. B, Condens. Matter*, vol. 405, no. 14, pp. 2925–2929, Jul. 2010.

[133] T. Liu, C. Zhou, and S. Xiao, "Gain-assisted critical coupling for enhanced optical absorption in graphene," *Nanotechnology*, vol. 32, no. 20, pp. 1–6, 2021.

[134] J. Wang, D. Han, A. Chen, Y. Dai, M. Zhou, X. Hu, Z. Yu, X. Liu, L. Shi, and J. Zi, "Using active gain to maximize light absorption," *Phys. Rev. B, Condens. Matter*, vol. 96, no. 19, pp. 1–5, Nov. 2017.

[135] J. Chen, W. Ding, X.-M. Li, X. Xi, K.-P. Ye, H.-B. Wu, and R.-X. Wu, "Absorption and diffusion enabled ultrathin broadband metamaterial absorber designed by deep neural network and PSO," *IEEE Antennas Wireless Propag. Lett.*, vol. 20, no. 10, pp. 1993–1997, Oct. 2021.

[136] H. Zhu, J. Wang, Y. Sun, and X.-L. Wu, "An improved genetic algorithm for optimizing EBG structure with ultra-wideband SSN suppression performance of mixed signal systems," *IEEE Access*, vol. 8, pp. 26129–26138, 2020.

[137] C. C. Akturk, M. Karaaslan, E. Ozdemir, V. Ozkaner, F. Dincer, M. Bakir, and Z. Ozer, "Chiral metamaterial design using optimized pixelated inclusions with genetic algorithm," *Opt. Eng.*, vol. 54, no. 3, pp. 1–7, 2015.

[138] Y. Wang, J. Wu, Z. Wang, C. Huang, H. Y. Fu, and Q. Li, "Optimization of epsilon-near-zero multilayers for near-perfect light absorption using an enhanced genetic algorithm," *IEEE Photon. J.*, vol. 13, no. 5, pp. 1–10, Oct. 2021.

[139] D. Li, L. Zigoneanu, B.-I. Popa, and S. A. Cummer, "Design of an acoustic metamaterial lens using genetic algorithms," *J. Acoust. Soc. Amer.*, vol. 132, no. 4, pp. 2823–2833, Oct. 2012.

[140] A. Mayer, H. Bi, S. Griesse-Nascimento, B. Hackens, J. Loicq, E. Mazur, O. Deparis, and M. Lobet, "Genetic-algorithm-aided ultra-broadband perfect absorbers using plasmonic metamaterials," *Opt. Exp.*, vol. 30, no. 2, pp. 1167–1181, 2022.

[141] D. I. Karatzidis, N. V. Kantartzis, G. G. Pyrialakos, T. V. Yioultsis, and C. S. Antonopoulos, "Genetic optimization with mixed-order prism macroelements for 3-D metamaterial multilayered structures," *IEEE Trans. Magn.*, vol. 55, no. 6, pp. 1–4, Jun. 2019.

[142] R. Eberhart and J. Kennedy, "New optimizer using particle swarm theory," in *Proc. Int. Symp. Micro Mach. Hum. Sci.*, 1995, pp. 39–43.

[143] J. Kennedy and R. Eberhart, "Particle swarm optimization," *Tsinghua Sci. Technol.*, vol. 21, no. 2, pp. 221–230, 1995.

[144] D. G. Y. Rahmat-Samii and J. Robinson, "Particle swarm optimization (PSO): A novel paradigm for antenna designs," *Radio Sci. Bull.*, vol. 305, no. 305, pp. 14–22, 2003.

[145] B. Choudhury, S. Manickam, and R. M. Jha, "Particle swarm optimization for multiband metamaterial fractal antenna," *J. Optim.*, vol. 2013, pp. 1–8, Apr. 2013.

[146] J. A. Bossard, D.-H. Kwon, Y. Tang, D. H. Werner, and T. S. Mayer, "Low loss planar negative index metamaterials for the mid-infrared based on frequency selective surfaces," in *Proc. IEEE Antennas Propag. Soc. Int. Symp.*, Jun. 2007, pp. 2873–2876.

[147] J. A. Bossard, S. Yun, Y. Tang, D. H. Werner, and T. S. Mayer, "Genetic algorithm synthesis of low-loss multi-layer negative index metamaterial stacks for the mid-infrared," in *Proc. 29th URSI General Assem.*, 2008, pp. 9–16.

[148] J. A. Bossard, S. Yun, D. H. Werner, and T. S. Mayer, "Synthesizing low loss negative index metamaterial stacks for the mid-infrared using genetic algorithms," *Opt. Exp.*, vol. 17, no. 17, 2009, Art. no. 14771.

[149] D. H. Kwon and D. H. Werner, "Low-index metamaterial designs in the visible spectrum," *Opt. Exp.*, vol. 15, no. 15, pp. 9267–9272, 2007.

[150] P. Y. Chen, C. H. Chen, H. Wang, J. H. Tsai, and W. X. Ni, "Synthesis design of artificial magnetic metamaterials using a genetic algorithm," *Opt. Exp.*, vol. 16, pp. 12806–12818, Aug. 2008.

[151] W. Xu and W. Wang, "Topology optimization of multilayer left-handed material based on the genetic algorithm," *Waves Random Complex Media*, vol. 23, no. 1, pp. 11–23, Feb. 2013.

[152] Z. Liu, U. K. Chettiar, A. V. Kildishev, V. M. Shalaev, D.-H. Kwon, Z. Bayraktar, and D. H. Werner, "Optical negative index metamerials with low losses: Nature-inspired methods for optimal design," in *Proc. Photonic Metamater., From Random Periodic*, 2007, pp. 1–3.

BASHAR A. F. ESMAIL (Member, IEEE) received the B.Eng. degree (Hons.) in electrical engineering (telecommunications) from Ibb University, Yemen, in 2008, and the M.Eng. and Ph.D. degrees in electrical engineering from Universiti Tun Hussein Onn Malaysia, Malaysia, in 2017 and 2021, respectively. In 2021, he joined as a Postdoctoral Researcher at the Faculty of Engineering, School of Electrical Engineering, Universiti Teknologi Malaysia, Johor, Malaysia. He is currently working as a Postdoctoral Researcher with the Engineering Optimization and Modeling Center (EOMC), Department of Electrical Engineering, Reykjavík University, Iceland. His research interests include the areas of design of metamaterial structures, millimeter wave antenna, MIMO, and reconfigurable antennas.

SLAWOMIR KOZIEL (Fellow, IEEE) received the M.Sc. and Ph.D. degrees in electronic engineering from the Gdańsk University of Technology, Poland, in 1995 and 2000, respectively, and the M.Sc. degrees in theoretical physics and in mathematics and the Ph.D. degree in mathematics from the University of Gdańsk, Poland, in 2000, 2002, and 2003, respectively. He is currently a Professor with the Department of Engineering, Reykjavík University, Iceland. His research interests include CAD and modeling of microwave and antenna structures, simulation-driven design, surrogate-based optimization, space mapping, circuit theory, analog signal processing, evolutionary computation, and numerical analysis.

STANISLAW SZCZEPANSKI received the M.Sc. and Ph.D. degrees in electronic engineering from the Gdańsk University of Technology, Poland, in 1975 and 1986, respectively. In 1986, he was a Visiting Research Associate with the Institut National Polytechnique de Toulouse (INPT), Toulouse, France. From 1990 to 1991, he was at the Department of Electrical Engineering, Portland State University, Portland, OR, USA, on a Kosciuszko Foundation Fellowship. From August to September 1998, he was a Visiting Professor with the Faculty of Engineering and Information Sciences, University of Hertfordshire, Hatfield, U.K. He is currently a Professor with the Department of Microelectronic Systems, Faculty of Electronics, Telecommunications and Informatics, Gdańsk University of Technology. He has published more than 160 articles and holds three patents. His teaching and research interests include circuit theory, fully integrated analog filters, high-frequency transconductance amplifiers, analog integrated circuit design, and analog signal processing.

HUDA A. MAJID (Member, IEEE) received the Ph.D. degree in electrical engineering from Universiti Teknologi Malaysia (UTM). He worked as a Postdoctoral Fellow with UTM for a period of one year. He is currently a Lecturer with the Faculty Engineering Technology, Universiti Tun Hussein Onn Malaysia (UTHM), Batu Pahat, Johor. He has published over 100 papers in journals and conferences. His research interests include planar and flexible antennas, array antennas, reconfigurable antennas, metamaterial, and RF microwave and mm-wave devices.